

Article

Phytonanofabrication of Copper Oxide from *Albizia saman* and Its Potential as an Antimicrobial Agent and Remediation of Congo Red Dye from Wastewater

Nisha Choudhary ^{1,*}, Jaimina Chaudhari ¹, Vidhi Mochi ¹, Pritee Patel ¹, Daoud Ali ², Saud Alarifi ², Dipak Kumar Sahoo ³, Ashish Patel ^{1,*} and Virendra Kumar Yadav ^{1,*}

¹ Department of Life Sciences, Hemchandracharya North Gujarat University, Patan 384265, Gujarat, India; jaiminachaudhari976@gmail.com (J.C.); mochividhi23@gmail.com (V.M.); patelpriti9800@gmail.com (P.P.)

² Department of Zoology, College of Science, King Saud University, P.O. Box 2455, Riyadh 11451, Saudi Arabia

³ Department of Veterinary Clinical Sciences, College of Veterinary Medicine, Iowa State University, Ames, IA 50011, USA; dsahoo@iastate.edu

* Correspondence: nishanaseer03@gmail.com (N.C.); uni.ashish@gmail.com (A.P.); yadava94@gmail.com (V.K.Y.)

Abstract: Metal nanoparticle fabrication through plant-based green methods is considered the gold standard among the various synthesis techniques owing to its simplicity, eco-friendliness, ease of use, and the huge diversity of plant species. Copper nanoparticles (CuONPs) have proven their potential in the fields of medicine, agriculture, pharmaceuticals, and catalysis, and are being synthesized using various physicochemical and biological methods. Here, the authors have reported on the first-ever use of *Albizia saman* leaf extract for the development of CuONPs. Phytochemical analysis of the methanolic extracts of the plant exhibited the presence of phenols (32.31%), tannins (12.27%), and flavonoids (16.72%). The phytonutrients existing in leaf extract successfully reduced the copper salt in the CuONPs. A detailed investigation of the synthesized CuONPs was performed using advanced instruments. The UV-Vis spectra exhibited an absorbance peak at 290 nm, while the X-ray diffraction pattern (XRD) revealed that the average crystallite size was about 29.86 nm. Dynamic light scattering (DLS) revealed that the average hydrodynamic size of the CuONPs was 72.3 nm in diameter, while its zeta potential was -0.49 , with a negative polarity. Fourier transform infrared spectroscopy showed the major bands in the region of 400 to 1000 cm^{-1} , suggesting the formation of CuONPs, while the band in the region of 1100 to 2600 cm^{-1} shows the association of plant molecules with the phytonanofabricated CuO particles. Transmission and scanning electron microscopy showed the spherical shape of the CuONPs, whose size was about 20 – 50 nm. The phytonanofabricated CuO exhibited antibacterial activity by forming a zone of inhibition (ZOI) against *Escherichia coli*, *Staphylococcus aureus*, and *Candida albicans*. The removal efficiency of the CuONPs was 33.33% for Congo Red dye. The removal efficiency of the phytonanofabricated CuO for CR dye was reduced to 16% after the 4th cycle.

Keywords: nano bioremediation; photosynthesis; antimicrobial activity; percentage removal; copper oxide



Citation: Choudhary, N.; Chaudhari, J.; Mochi, V.; Patel, P.; Ali, D.; Alarifi, S.; Sahoo, D.K.; Patel, A.; Yadav, V.K. Phytonanofabrication of Copper Oxide from *Albizia saman* and Its Potential as an Antimicrobial Agent and Remediation of Congo Red Dye from Wastewater. *Water* **2023**, *15*, 3787. <https://doi.org/10.3390/w15213787>

Academic Editor: Manuel Toledo Padrón

Received: 7 October 2023

Revised: 25 October 2023

Accepted: 27 October 2023

Published: 29 October 2023



Copyright: © 2023 by the authors. Licensee MDPI, Basel, Switzerland. This article is an open access article distributed under the terms and conditions of the Creative Commons Attribution (CC BY) license (<https://creativecommons.org/licenses/by/4.0/>).

1. Introduction

Nano metals such as silver [1], gold, copper, nano zero-valent iron (NZVI), platinum [2], palladium [3], etc., and metallic nano-oxide particles, for instance, oxides of Cu, Mg, Fe, Ti, Si, Zn, etc. [4–9], are the most versatile nanocrystalline materials. These metallic and metal oxide nanoparticles (NPs) have found widespread applications across diverse fields, such as catalysis (electro and photocatalysts) [10], medicine (antimicrobial agents and drug carriers for drug delivery) [11], and environmental remediation (waste treatment) [12–14] due to their remarkable characteristics. The uniqueness of these NPs lies

in their nano size, higher surface area, higher reactivity, higher bioavailability, lower toxicity, specific targeting, and precise release [15,16]. Amongst numerous metal nano-oxide particles, copper oxide nanoparticles (CuONPs) have attracted significant research attention in recent years owing to their unique properties and comprehensive applications [17,18].

Copper was the first metal antimicrobial agent recognized by the US Environmental Protection Agency. Copper has shown effective neutralizing effects against viruses such as poliovirus, HIV 1, bronchitis viruses, etc. [19,20]. It has oxidation-reducing properties, due to which it can be utilized as an acceptor or donor of electrons in enzymes and can efficiently act as a catalyst for certain reactions [21]. These nanoparticles can be impregnated into protective wear, filters, and facial masks. Copper-based coatings have revealed bactericidal activities against important human pathogens [22–25]. CuONPs are effective in adsorbing, degrading, or immobilizing contaminants, thereby reducing environmental hazards [26]. The biocompatibility of these nanoparticles reduces the risk of toxicity, making them an attractive option for medical applications. They have also found applications in the area of agriculture to enhance crop yield and tolerance against abiotic stress, such as drought [27–29].

The properties of CuONPs depend on the methods through which they are synthesized. Laser ablation, physical vapor deposition, sol–gel [30], electrochemical [31], polymer dispersion, solvent evaporation [29,32], ultrasonication [33], microwave [34], hydrothermal, solvent extraction, or diffusion are some of the physicochemical approaches used for developing copper and CuONPs. Apart from these methods, green methods for synthesis are gaining interest because of the lower price and toxicity, easiness, and eco-friendliness of the synthesis mechanism [35]. The plant-based biosynthetic approach for the formation of nano metals and metal nano-oxide particles is an economically profitable and environmentally friendly fabrication method [36,37]. Additionally, the plant-based synthesis approach offers a greener alternative to traditional remediation methods as nano metals and metal nano-oxide particles are derived from renewable resources and require less energy for synthesis [38].

Plants are rich sources of numerous phytoconstituents such as terpenoids, saponins, glycosides, tannins, steroids, and flavonoids that can act as reducing and capping agents [39]. Moreover, these phytochemicals stabilize the nanoparticles developed using the nucleation method [40]. *Albizia saman*, a flowering tree from the Fabaceae family commonly known as the “Rain tree”, has high nutritional values and nitrogen-fixing capability [39]. *A. saman* displays numerous bio-active compounds that possess several therapeutic properties like antibacterial, antifungal, insecticidal, analgesic, antioxidant, antidiabetic, cytotoxic, and anti-ulcer activities [41–43].

Earlier, several attempts were made to synthesize CuONPs using different species of *Albizia*, for instance, Jayakumari and colleagues used the leaf extracts of *A. lebeck*, while Ramya and colleagues used *A. amara* for the development of CuONPs. To date, no attempts have been made to synthesize CuONPs using *A. saman*.

Congo Red (CR) dye is used in paints, pigments, textiles, staining tissues, and the pharmaceutical industry [44]. CR dye affects different living beings in different ways, for instance, it may be carcinogenic, mutagenic, allergy causing, or organ damaging for humans, may cause infertility and toxicity in certain aquatic organisms, and may increase COD levels in water bodies, which is an indicative parameter of chemical pollution in water systems [45,46].

In the present research work, phytonanofabrication of CuO was performed utilizing leaf extract of *A. saman* for the very first time. One of the objectives was to characterize the formulated CuONPs using analytical instruments to identify their detailed features. Further, the antimicrobial properties of the synthesized CuONPs were assessed against *Staphylococcus aureus*, *Escherichia coli*, and *Candida albicans*. Finally, one of the main objectives was to assess the adsorption efficiency of the phytonanofabricated CuO particles for the elimination of Congo Red dye from the contaminated water.

2. Materials and Methods

A. saman leaves were plucked from the university premises of HNGU in Patan district of Gujarat state in India. Copper sulfate (99.0% pure) was purchased from SD Fine Chem Limited, Mumbai, India. For the analysis of the antimicrobial activity of CuONPs, microbial cultures of *S. aureus*, *E. coli*, and *C. albicans* were procured from the GSBTM, Gandhinagar, Gujarat, India, while Congo Red ($C_{32}H_{22}N_6Na_2O_6S_2$) was purchased from SRL, Maharashtra, India. Sterile double-distilled water (ddw) was utilized for solution preparation for the investigations.

2.1. Metal Precursor Solution Preparation

About 0.039 g of $CuSO_4 \cdot 5H_2O$ was weighed and added to 100 mL of ddw in a conical, 250 ml flask. The flask was capped using a cotton plug, and covered with aluminum foil until use.

2.2. Preparation of *A. saman* Leaf Extract

The collected leaves of *A. saman* were further processed in the university laboratory for the preparation of CuONPs. As an initial step, dust particles and other impurities were removed from the surface of the leaves by washing them 2–3 times with tap water followed by final washing with ddw. The washed leaves were shade-dried by placing them on blotting paper in the laboratory at room temperature for 24 h. The dried leaves were crushed using a mortar and pestle. To a beaker containing 100 mL of 50% methanol (methanol and water at a ratio of 1:1), 25 g of dried and powdered leaves was added and kept at RT for 24 h. To obtain the extract, this mixture was separated using Whatman filter paper no. 42. Further, centrifugation of the mixture was conducted at 8000 rpm for 5 min. The collected filtrate was used as the extract, while the residue containing plant cellular macromolecules was discarded. This suspension obtained from the centrifugation was employed further for reducing copper salt and capping the CuONPs [47,48].

2.3. Quantitative Analysis of Phytochemical Content and Antioxidant Activity of *A. saman*

2.3.1. Total Phenolics

The total concentration of phenolics was evaluated as per the modified Folin–Ciocalteu colorimetric technique described by Singleton and Rossi [49,50]. About 0.5 mL of the extracted solvent was diluted with ddw (4.50 mL), to which 0.5 mL of Folin–Ciocalteu's reagent was added. After mixing the mixture for 10 min, 5 mL of 7% Na_2CO_3 (*w/v*) was added for its neutralization. Further, the solution was incubated under dark conditions for 90 min, after which UV-Vis measurement was taken at 765 nm. The expression of the results was analyzed on a weight basis (DW) as mg gallic acid equivalent/g (mg GAE/g DW) of the sample.

2.3.2. Total Flavonoid Content (TFC)

The estimation of the TFC was performed in line with the protocol reported by Chang and their group, using the $AlCl_3$ colorimetric method [51]. The $AlCl_3$ colorimetric technique was used to estimate the flavonoid quantity in the extract. The preparation of the reaction mixture was conducted by mixing (0.5 mL extract 1.50 mL ddw + 0.5 mL 10% (*w/v*) $AlCl_3$ + 0.1 mL 1 M potassium acetate). The above reaction mixture was diluted with 2.8 mL ddw and finally placed at 22 °C for 35 min. To obtain the data, the absorbance was taken at 415 nm using spectrophotometry, and the expression of the data was conducted in mg quercetin equivalent/grams of dried weight (mg QE/g).

2.3.3. Total Tannin Content

The estimation of the total tannin content was conducted using the protocol of Ram and Mehrotra (1993), with minor modifications [52]. A mixture of different solvents of (5 mL) was developed through mixing [0.5 mL Folin–Dennis reagent + 1 mL Na₂CO₃ (saturated solution)]. Further, the above mixture was kept at 22 °C for 20 min, and the measurement of the blue color was performed at 700 nm. The data were expressed as mg tannic acid equivalents/grams of dried weight (dw).

2.3.4. ABTS Free Radical Scavenging (FRS) Assay

The measurement of total antioxidant activity was conducted using an improved Azinobis (ethylbenzothiazoline 6-sulphonic acid) radical scavenging (ABTS) process, with slight modifications [53], as described below in Figure 1.

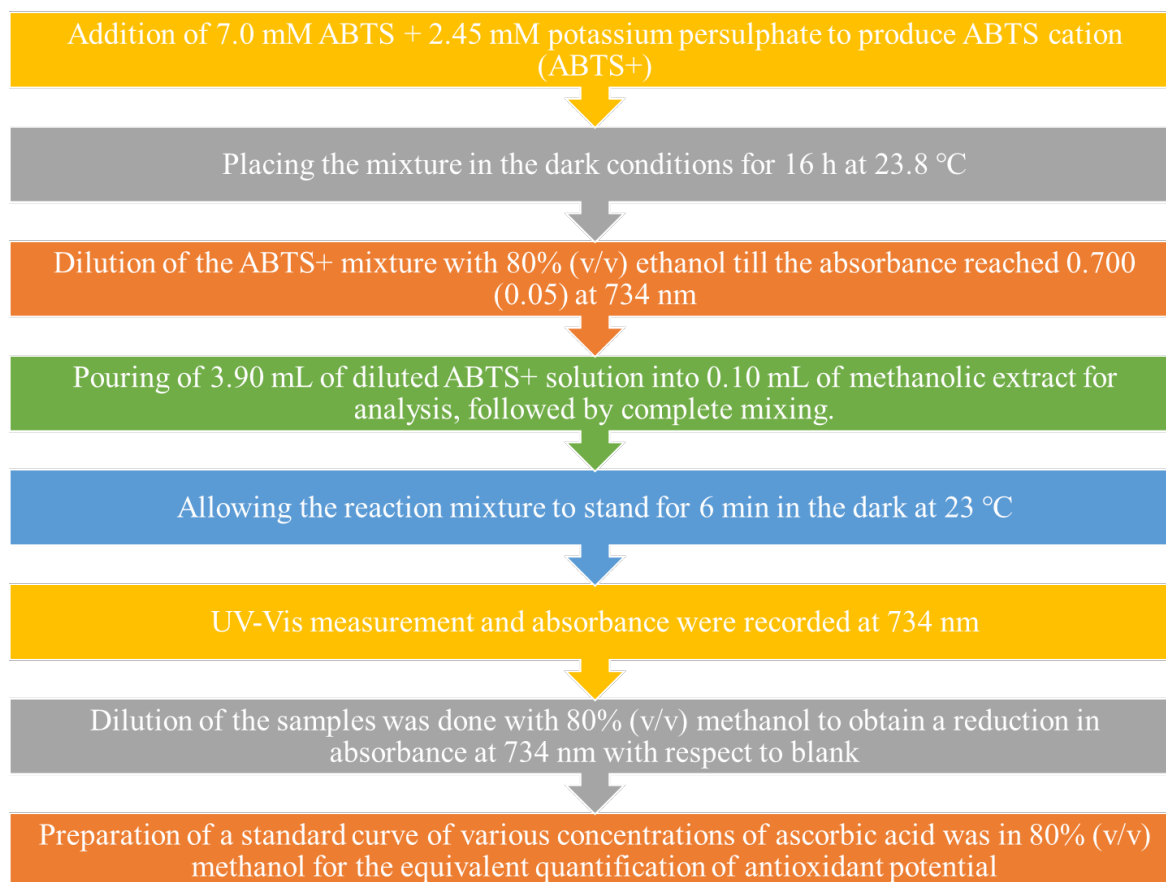


Figure 1. Steps involved in the ABTS-FRS assay.

2.3.5. Diphenyl-2-Picryl-Hydrazyl (DPPH) FRS Assay

The DPPH assay was carried out according to the protocol suggested by Brand-William et al. (1995), with certain changes. The detailed steps are shown below in Figure 2 [54].

2.3.6. Ferric Reducing Antioxidant Power (FRAP) Assay

FRAP assay was performed following the protocol reported by Benzie and Strain (1996), with certain changes [55], as shown below in Figure 3.

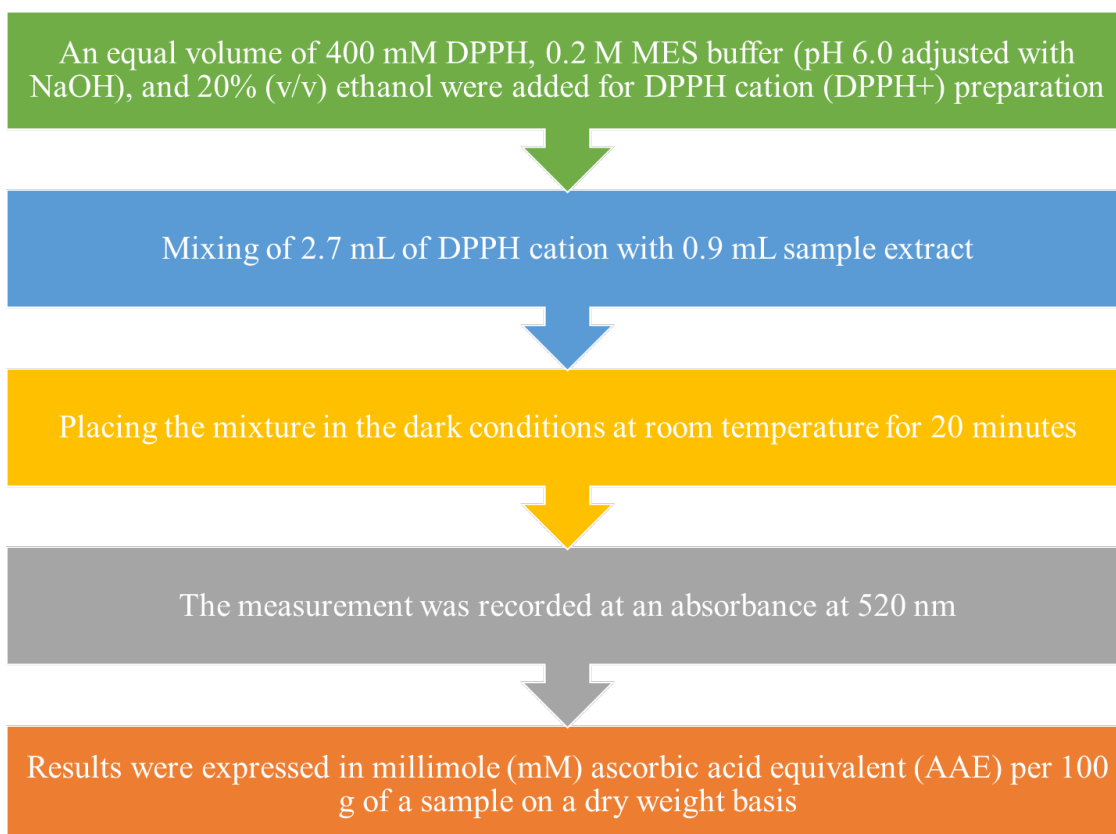


Figure 2. Steps involved in the DPPH assay.

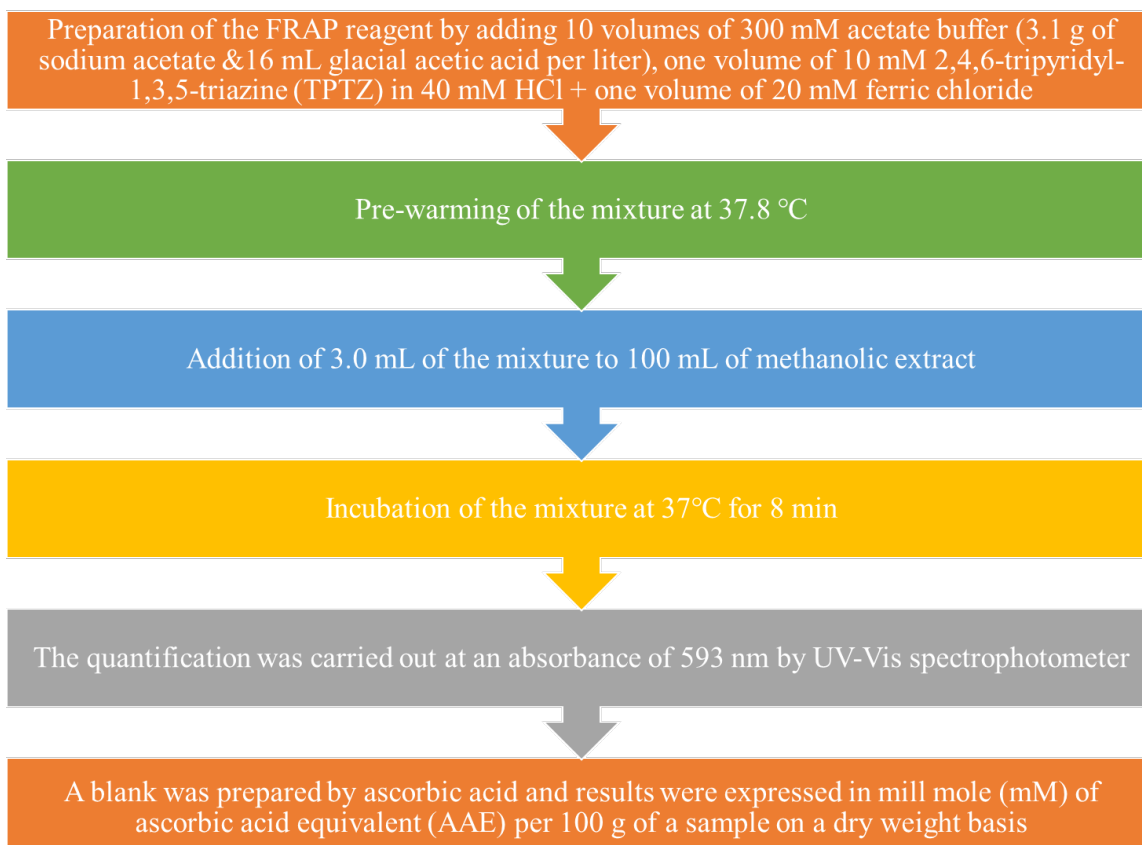


Figure 3. Steps involved in the FRAP assay.

2.4. Photosynthesis of CuONPs from CuSO₄

About 80 mL of CuSO₄ solution was poured into a 250 mL beaker, which was then placed on a magnetic stirrer at 250 rpm and heated at 50 °C. About 20 mL of freshly prepared extracts from leaves were poured into the precursor solution. The stirring was continued until the color changed from green to dark brown. The mixture was then left on the magnetic stirrer at 50 °C for 24 h, followed by centrifugation at 8000 rpm for 10 min in order to obtain the CuONPs in the form of precipitate at the bottom of the tube. The obtained pellet was washed thrice with sterile ddw in order to eliminate any impurities attached to the particles. Finally, the obtained pellet was transferred to a Petri plate and was oven-dried at 80 °C overnight. The dried powder was then calcined in an electrical muffle furnace at 500 °C for 5 h. A brown-colored powder of CuO was thus obtained, which was confirmed to be CuONPs through analysis using various sophisticated instruments.

2.5. Batch Adsorption Experiments

For the CR dye removal study, batch experiments were carried out for the adsorption of CR on CuONPs. In this study, the effect of contact time on the adsorption of CR dye molecules was studied. In the experimental set-up, a 250 mL beaker containing 50 ppm of 100 mL of dye solution with a pH of 8 was kept on a magnetic stirrer at a revolution speed of 200 rpm. About 50 mg of CuONPs was added to the CR solutions. The mixtures were stirred continuously using a magnetic stirrer at 200 rpm for 60 min. After a regular interval of 5 min, an aliquot of 3 mL solution was taken out and examined for remaining CR dye concentration using a UV-visible double beam spectrophotometer ($\lambda_{\max} = 498$ nm). The percentage removal (%R) of CR dye and adsorption capacity of CuONPs at any time (q_t) and at equilibrium (q_e) were evaluated using the following formulas [44,56].

$$\% \text{ Removal} = \frac{A_0 - A_t}{A_0} \times 100 \quad (1)$$

$$q_t \text{ (mg/g)} = \frac{(A_0 - A_t)V}{M} \quad (2)$$

$$q_e \text{ (mg/g)} = \frac{(A_0 - A_e)V}{M} \quad (3)$$

where,

A_0 = initial conc. of CR dye (mg/L)

A_t = conc. of CR dye at a specific time, t (mg/L)

A_e = conc. of CR dye at equilibrium (mg/L)

V = volume of CR dye solution (L)

M = mass of CuONPs (g)

2.6. Antimicrobial Activity of Phytonanofabricated CuO

The phytofabricated CuONPs were assessed for their antimicrobial potential against *E. coli* and *S. aureus*, measured on nutrient agar media, while the antifungal activity against *C. albicans* (yeast) was conducted on potato dextrose agar (PDA) utilizing the disc diffusion technique. A stock solution (0.1 mg per mL) of CuONPs was prepared in ddw. A filter paper disc was placed into this solution and then, the sonication of the mixture was conducted for 5 min. In this way, CuONPs were loaded onto the disc surface. The assessment was performed by applying a microbial inoculum to a nutrient agar plate and potato dextrose agar (PDA) using the swab culture technique. The inoculated Petri plates were incubated at 37 °C for one day; thereafter, the Petri plates were examined for the formation of a zone of inhibition (ZOI).

3. Characterization of CuONPs

An FTIR investigation was conducted to identify the various functional groups attached to the CuONPs. A solid KBr pellet technique was applied for the FTIR analysis, where about 2 mg CuONPs + 98 mg of KBr was taken. The investigation was conducted using SP 65 (Perkin Elmer, Waltham, MA, USA) in the mid-IR region 400–4000 cm^{-1} , with a resolution of 1 nm. The particle size distribution (PSD) of the CuONPs was examined through dynamic light scattering (DLS), for which aqueous solution was prepared by dispersing 1–2 mg of powder in the sterile distilled water and sonicated for 10 min in an ultrasonicator (Sonar, Barcelona, Spain, 40 kHz). The sonication-dispersed nanoparticle solution was used for the DLS at room temp. and UV-visible measurement was conducted in the region of 200–800 nm using a Shimadzu UV-1900i double-beam spectrophotometer (Japan). For FESEM analysis, about 0.5 mg of CuONPs was taken on the carbon tape, which, in turn, was attached to the aluminum stub. Further, the CuONPs were subjected to Au-sputtering before FESEM analysis. The external size and shape of the phytonanofabricated CuO were examined utilizing Nova NanoSEM 450 FEI (USA), while the elemental investigation was carried out using Bruker's EDX analyzer attached with FESEM.

4. Results and Discussion

4.1. Phytochemical Analysis of *A. saman* Methanolic Leaf Extract

The data obtained via phytochemical assay of the methanol extract of *A. saman* leaves indicated the presence of secondary metabolites such as phenols, tannins, and flavonoids (Table 1). The total phenolic content was about 32.31 mg GAE/g, the total tannin content was 12.27 mg TAE/g, whereas the total flavonoid content was 16.72 mg QE/g of the methanolic extract of *A. saman*. The results of the antioxidant activity evaluated by measuring FRAP, ABTS, and DPPH assay are presented in Figure 4.

Table 1. Total phenolic, tannin, and flavonoid content in methanol extract of *A. saman*.

S. No.	Secondary Metabolite	Conc. (mg/g)	Study by Anil et al. (Per/Gram)
1.	Phenols	32.31	
2.	Tannins	12.27	
3.	Flavonoids	16.72	2.12 mg

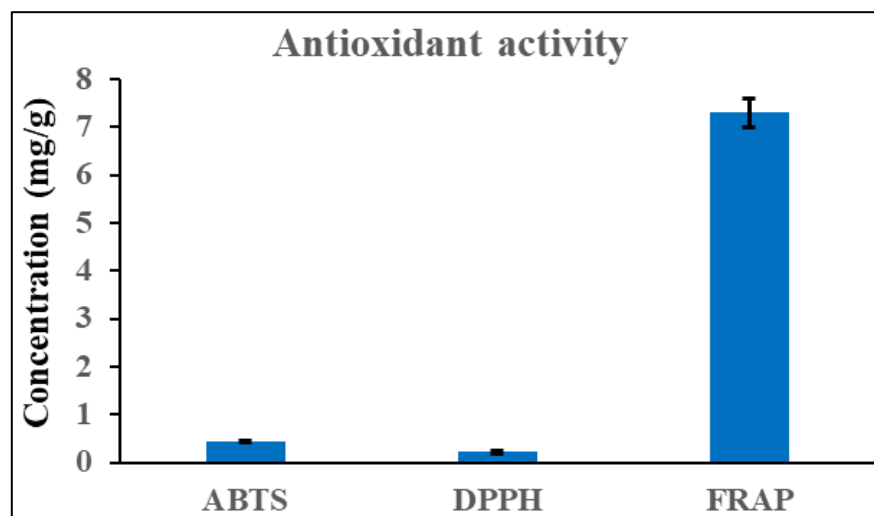


Figure 4. Phytochemical analysis of *A. Saman* leaf extract.

Previously, Venugopal also reported the phytochemical analysis of the methanolic extract of *A. saman*. Further, investigators have reported on DPPH assay, reducing power assay, and nitric oxide scavenging assay [57]. Anil and colleagues also investigated the phytochemical analysis (phenol content, tannin content, flavonoids, etc.) of the fruit pulp of *A. saman* (Jacq.) Merr. The investigators revealed that the flavonoids were about 2.2 mg/g in the fruit samples of *A. saman*. The presence of terpenoids and tannins along with catalase, oleic acid, etc. was also observed in the fruit sample [58].

4.2. Mechanism of Formation of CuONPs from *A. saman*

A. saman has numerous phytochemicals like tannins, flavonoids, and terpenoids in addition to several others. These phytochemicals have various functional groups through which these Cu^{2+} ions bind. Further, there is a formation of Cu^{2+} metal complexes which are reduced to form CuO seed particles. Further, these seed CuO particles then undergo aggregation and nucleation [59]. Earlier, a team of investigators suggested that the flavonoids in the leaf extract of *Solanum nigrum* release an H-atom, where there is a tautomeric change (enol to keto) via the reduction of $\text{Cu}(\text{NO}_3)_2$ to CuONPs. Due to this bioreduction, there is a color change of the medium i.e., from blue to brown [60]. A schematic representation is shown in Figure 5a, depicting the phytonanofabrication of CuO from the plant extract, while Figure 5b shows the mechanism of the formation of CuONPs from *E. globulus* leaf extract.

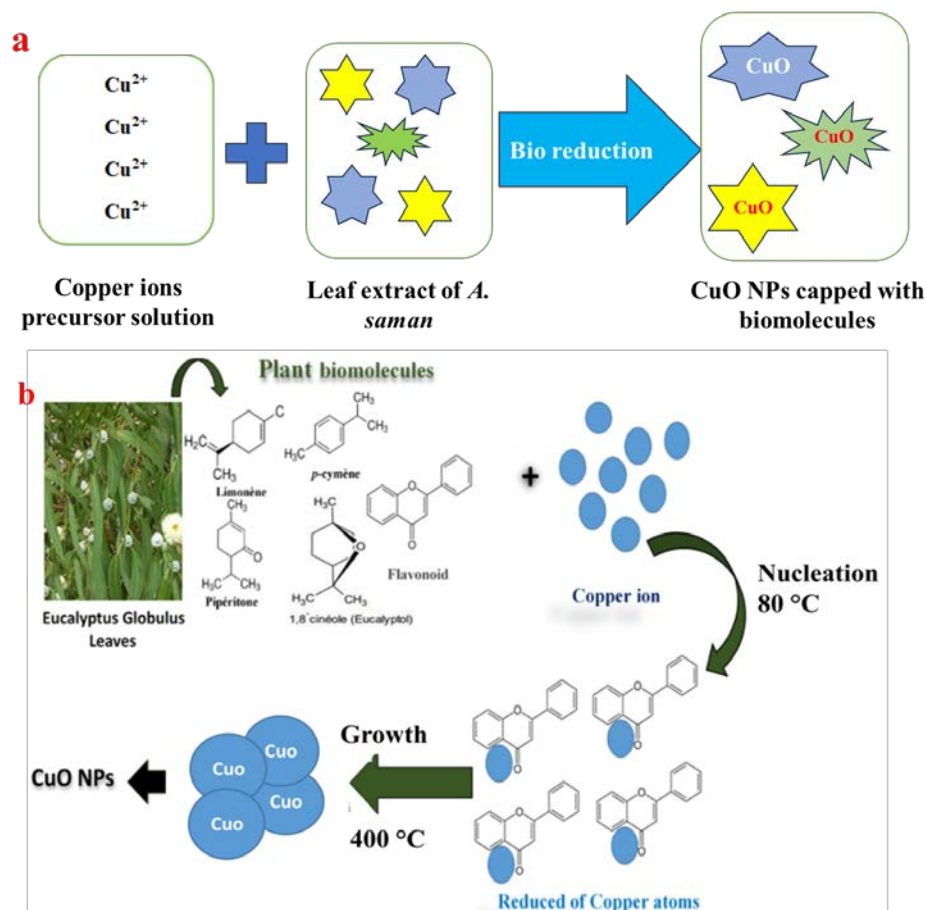


Figure 5. Mechanism of formation of CuONPs from the plant extract of *A. saman* (a) and *E. globulus* (b) [59].

4.3. PSD of CuONPs Using DLS

Figure 6 shows a typical PSD graph of the CuONPs, where the CuONPs exhibit particle size between 60 and 120 nm. The average hydrodynamic size of the phytosynthesized CuONPs was 72.30 nm (dm) and the zeta potential was -0.49 mV. The conductivity was about $22 \mu\text{S}/\text{cm}$, while mobility was $-0.04 \mu\text{s}/\text{V}/\text{cm}$. In addition to this, the synthesized CuONPs had a negative polarity, with a charge of about -0.01271 fC, which indicates the association of negatively charged molecules on the surface of the CuONPs. The obtained results were in good agreement.

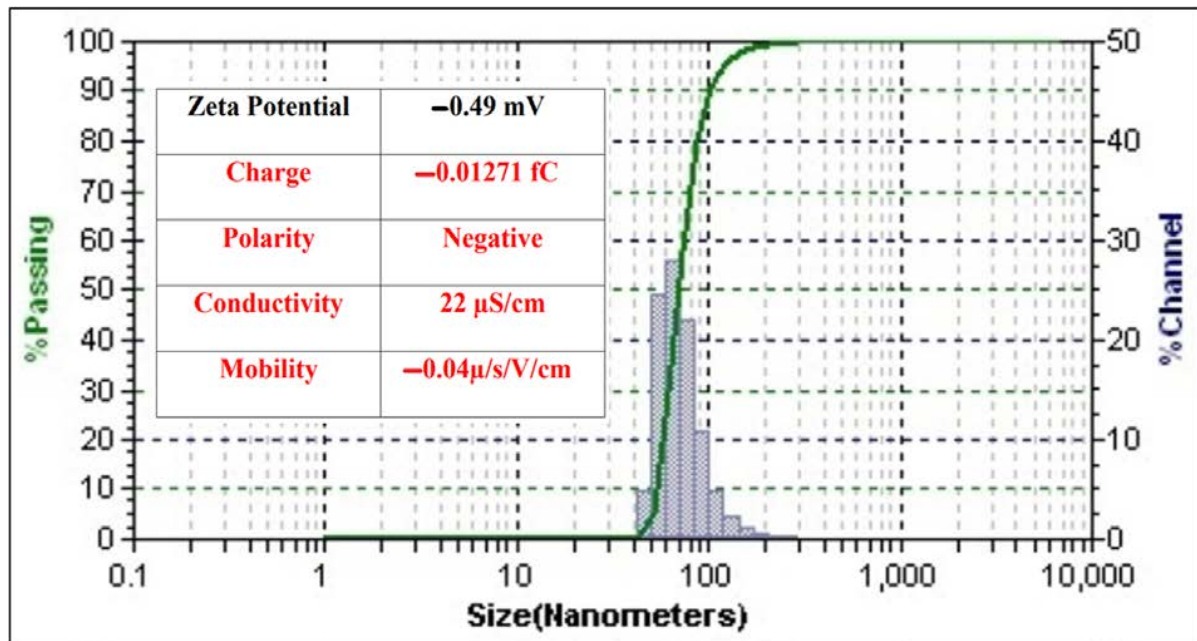


Figure 6. Particle size distribution graph of CuONPs synthesized by *A. saman*.

Earlier, Nazilu and colleagues synthesized CuONPs from the aqueous extracts of the whole *Parthenium hysterophorus* plant, performed the DLS, and obtained particles of sizes varying from 0 to 200 nm in diameter. There were two types of particles, i.e., smaller ones with a size in the range of 0–200 nm, and a large population of an average size <100 nm. The PDI was 0.3 or less, indicating that the individual particle size distribution was monodispersed. The DLS showed the polydisperse nature of the synthesized CuONPs, while SEM showed the monodisperse nature of the CuONPs [61].

Zahrah Alhalili (2022) obtained a hydrodynamic size of about 85.3 nm in diameter for the CuONPs synthesized from the *Eucalyptus globulus*, and the maximum particle size distribution was 81.92 nm. Moreover, the zeta potential was found to be -30 , which suggested the high stability of the particle in the solution. Earlier, investigators concluded that the average zeta potential of the CuONPs could vary from -20 to $+45$, depending on the pH between 2 and 12 [59]. Venkata and colleagues also synthesized CuONPs from *Solanum nigrum*, where the zeta potential was found to be -12.5 ± 3.59 mV at pH 6.8 and PDI was 0.445. The investigators suggested that the negative polarity might be due to the presence of negatively charged molecules on the surface of CuONPs, like OH, or due to the dissociation of acidic groups on the surface of the NPs after dispersing into the water.

4.4. UV-Visible Spectroscopic Analysis

Figure 7 presents the UV-Vis spectrum of crude leaf extract of the *A. saman* plant and CuONPs. A change in color suggests the phytonanofabrication of CuO, revealing an absorbance peak at 290 nm due to the surface plasmon resonance (SPR) [62]. Similar results were also obtained by a team led by Swathilakshmi for phytosynthesized CuONPs using *A. amara* [63]. Ramya and colleagues obtained a peak at 288 nm for the CuONPs synthesized

from the leaf extracts of *A. amara*. A group led by Jayakumari obtained an absorbance peak of 413 nm for the CuONPs formed using *A. lebbek*. Here, the investigators noticed a color change after 24 h of incubation, where the color change was due to the excitation of SPR of CuONPs [64]. The CuONPs formed in our study were in close agreement with previous results, which reported that CuONPs formed in the range of 200–350 nm.

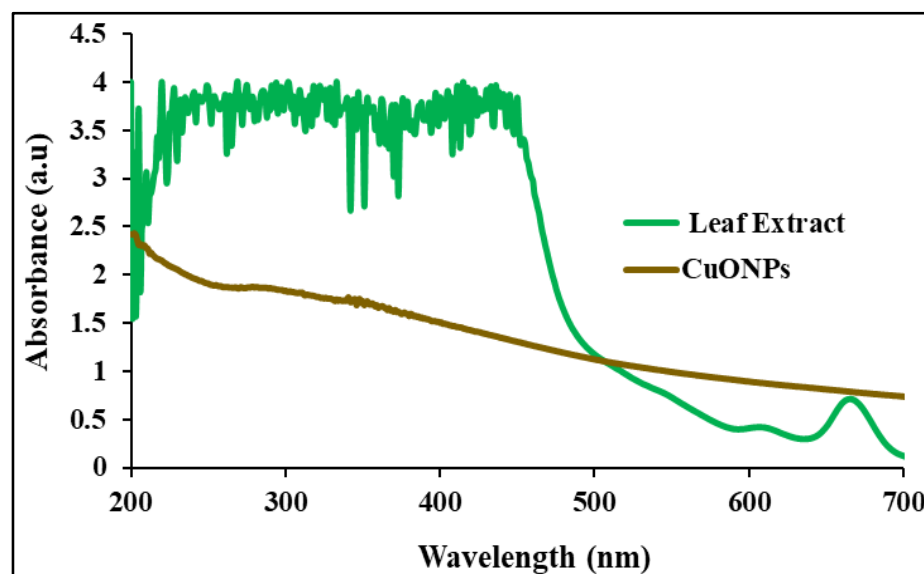


Figure 7. UV-Vis spectrum of *A. saman* leaf extract and CuONPs.

4.5. FTIR Analysis of CuONPs for the Identification of Functional Groups

FTIR measurement of CuONPs was performed in order to identify the attached biomolecules that acted as a capping and stabilizing agent. FTIR spectrum (Figure 8) of CuONPs was observed at 3616 cm^{-1} , 3153 , 2933 , 1652 , 1369 , 1155 , 1079 , 1020 , 611 , 545 , and 510 cm^{-1} . The band at 3616 and 3153 cm^{-1} could be attributed to the O-H stretching of alcohols and phenols. The band at 2933 cm^{-1} could be attributed to –NH bond stretching. The bands at 1652 cm^{-1} and 1369 cm^{-1} may be attributed to C=C and C-OH stretching vibrations. The band at 1155 cm^{-1} and 1079 cm^{-1} could correspond to the bending vibration of C-OH, whereas the bands at 1020 cm^{-1} and 611 cm^{-1} could correspond to C-O stretching vibrations in carboxylic acid and flavonoids. The bands at 545 cm^{-1} and 510 cm^{-1} could correspond to the Cu-O band vibrations, which confirms the synthesis of CuONPs. The major FTIR bands of the phytonanofabricated CuO are shown in Table 2.

Table 2. Functional group associated with phytofabricated CuONPs.

Wavenumber (cm^{-1})	Assigned Functional Groups	References
3607, 3165	O-H stretching of -OH group from phenols	[65]
2931	N-H bond stretching	[66]
1652	C=C stretching	[67]
1364	C-OH stretching vibrations	[68]
1161, 1079	C-OH bending vibrations	[69]
1020	C-O stretching vibrations in carboxylic acid and flavonoids	[69]
763		
611	C-O bending vibrations	[65]
545	Cu-O vibrations	[65]
510	Cu (II)-O bond vibrations	[65]

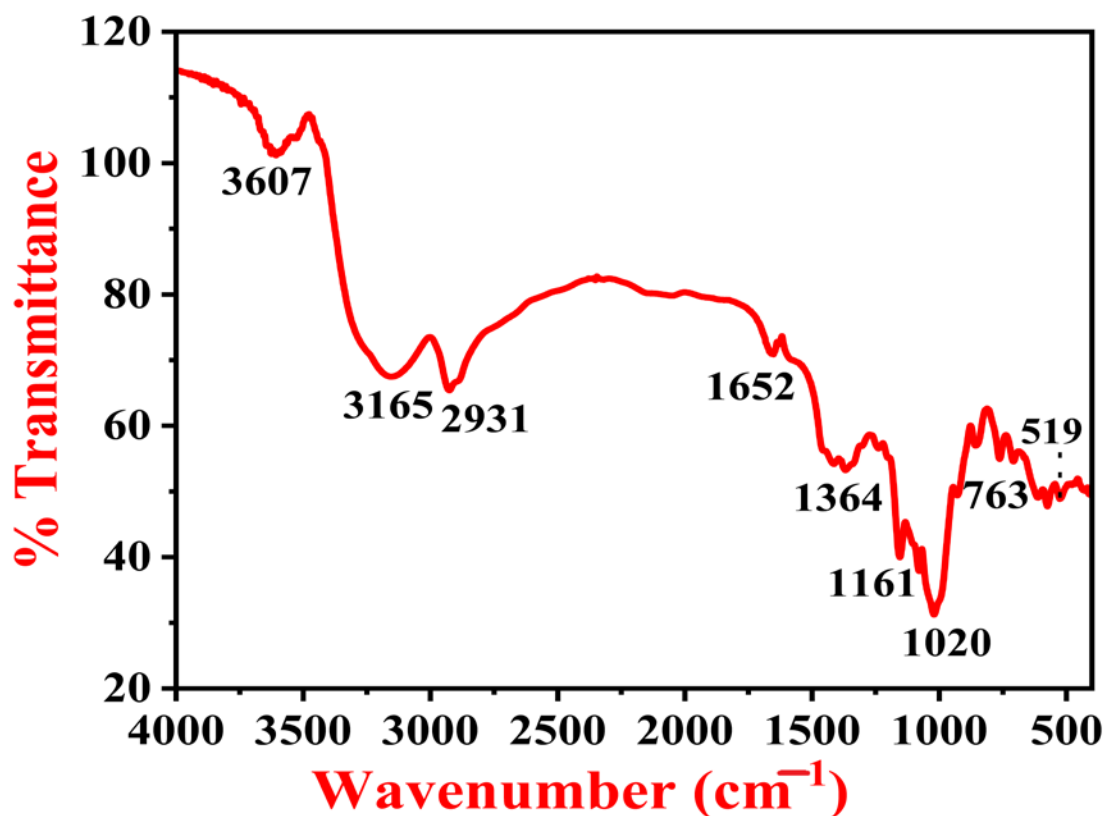


Figure 8. FTIR spectrum of CuONPs synthesized from the *A. saman*.

Earlier, Ramya and colleagues investigated both leaf extract and CuONPs synthesized from *A. samara* and obtained bands at 763 cm^{-1} , 1653 cm^{-1} , 2054 cm^{-1} , and 3445 cm^{-1} for the aqueous extract of leaves and for CuONPs at 535 cm^{-1} , 709 cm^{-1} , 1015 cm^{-1} , 1632 cm^{-1} , and 3393 cm^{-1} . The bands and their attributes were suggested as following 3393 cm^{-1} (OH stretching), 1632 cm^{-1} (OH bending), and 1015 cm^{-1} (C-O stretching), while a narrow band at 535 cm^{-1} was attributed to the Cu-O bond, confirming the formation of CuONPs [70].

4.6. Phase Identification and Crystallinity Determination of CuONPs Using XRD

A typical XRD pattern of CuONPs synthesized from the plant is depicted in Figure 9. It shows diffraction peaks at 16.9° , 36.4° , 43.3° , 50.4° , and 74.1° . A high-intensity, sharp peak is at 43.3° , which indicates the crystalline size of the synthesized CuONPs. Moreover, there are two more peaks—one at 50.4° and the other at 36.4° . Furthermore, there are two more small intensity peaks at 16.9° and 74.1° . In addition to this, there are no other peaks that suggests the purity of the phytonanofabricated CuO. The calculation of the crystallite size of the CuONPs was conducted using the Scherrer formula, as shown below in Equation (4):

$$D = \frac{k\lambda}{\beta \cos\theta} \quad (4)$$

where, D = crystalline size, k = constant (0.9), and β = full-width half maximum (FWHM) values of the diffracted peaks.

All the parameters used in the Scherrer equation were calculated using the highest intensity. The FWHM values and exact theta values were calculated using the Gaussian peak fits. The crystallite size of the synthesized CuONPs was 29.86 nm.

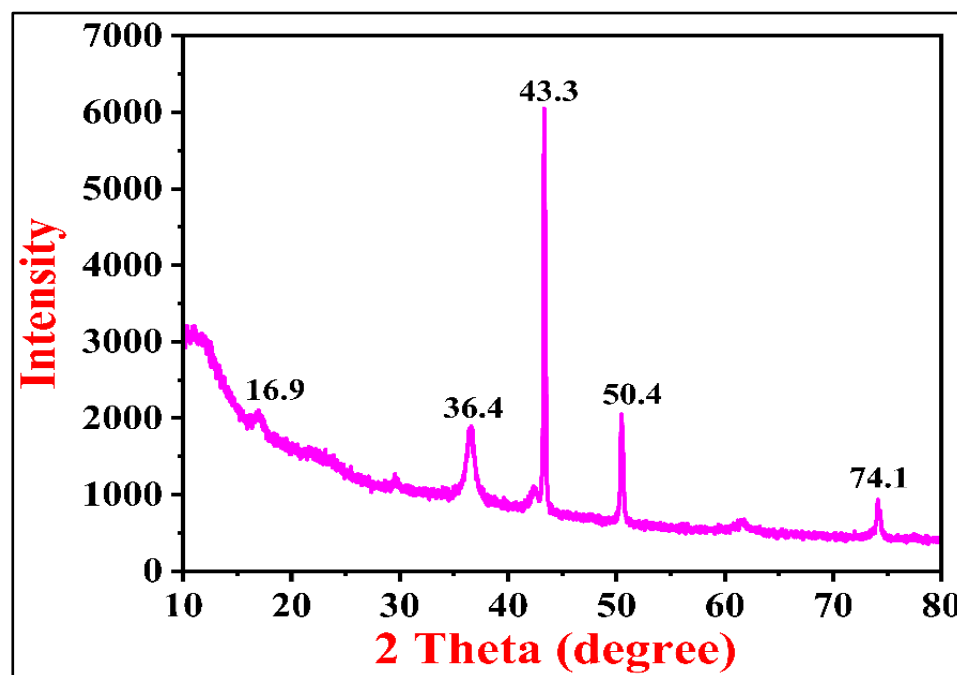


Figure 9. XRD pattern of CuONPs synthesized by *A. saman*.

The results of the current study were in close agreement with a previous study by Jayakumari and colleagues. The diffraction peaks along with their corresponding lattice planes of cubic CuONPs were obtained at $(2\theta) = 28.63$ (1 1 1), 32.08 (2 0 0), 44.48 (2 0 0), 46.12 (2 2 0), 61.68 (0 2 2), 64.52 (2 2 0), and 71.48° (3 1 1) [64]. Ramya and colleagues obtained diffraction bands for CuONPs synthesized from *A. amara* at $2\theta = 33.3, 35.4, 38.8, 48.7, 58.3, 61.8, 66.28,$ and 68.0 , which corresponds with the planes (110), (022), (111), (200), (202), (020), (202), and (022), respectively. The following group obtained an average crystallite size below 21 nm and a crystallite size of about 38.93 nm for the synthesized CuONPs [70].

4.7. Morphological Analysis of CuONPs

Figure 10a–d shows the FESEM micrographs of CuONPs synthesized from *A. saman* at different scales. Figure 10a shows the spherical-shaped CuONPs at 1 μ , while Figure 10b,c shows the CuONPs at 200 nm, depicting spherical-shaped CuONPs. Figure 10d shows the spherical-shaped CuONPs at 100 nm scale. The size of the particle varies from 30 to 90 nm, which is present as an individual and in aggregates. The size of the CuONPs synthesized by Ramya and colleagues from the aqueous extracts of *A. amara* was about 60–80 nm, which was roughly spherical in shape.

Figure 10e shows the EDS spot while Figure 10f depicts the EDS spectra and elemental table, respectively. The former exhibit peaks for C, O, and Cu. The presence of Cu indicates the formation of CuO, while the presence of carbon supports the association of plant organic compounds with the synthesized CuONPs. The EDX analysis of CuONPs indicates that they contain Cu (38.93%) and O (61.07%).

Previously, Jayakumarai and colleagues also reported the formation of spherical-shaped CuONPs from *A. lebeck*, whose size was below 100 nm [64]. The EDS analysis of the synthesized CuONPs showed peaks for only Cu and O, which were 34.78% (wt.%) and 65.22% (wt.%) [64]. The EDS analysis of CuONPs synthesized by Ramya and colleagues from *A. amara* revealed peaks for Cu and O, which were 78.07 (wt.%) and 21.93 (wt.%), respectively [70].

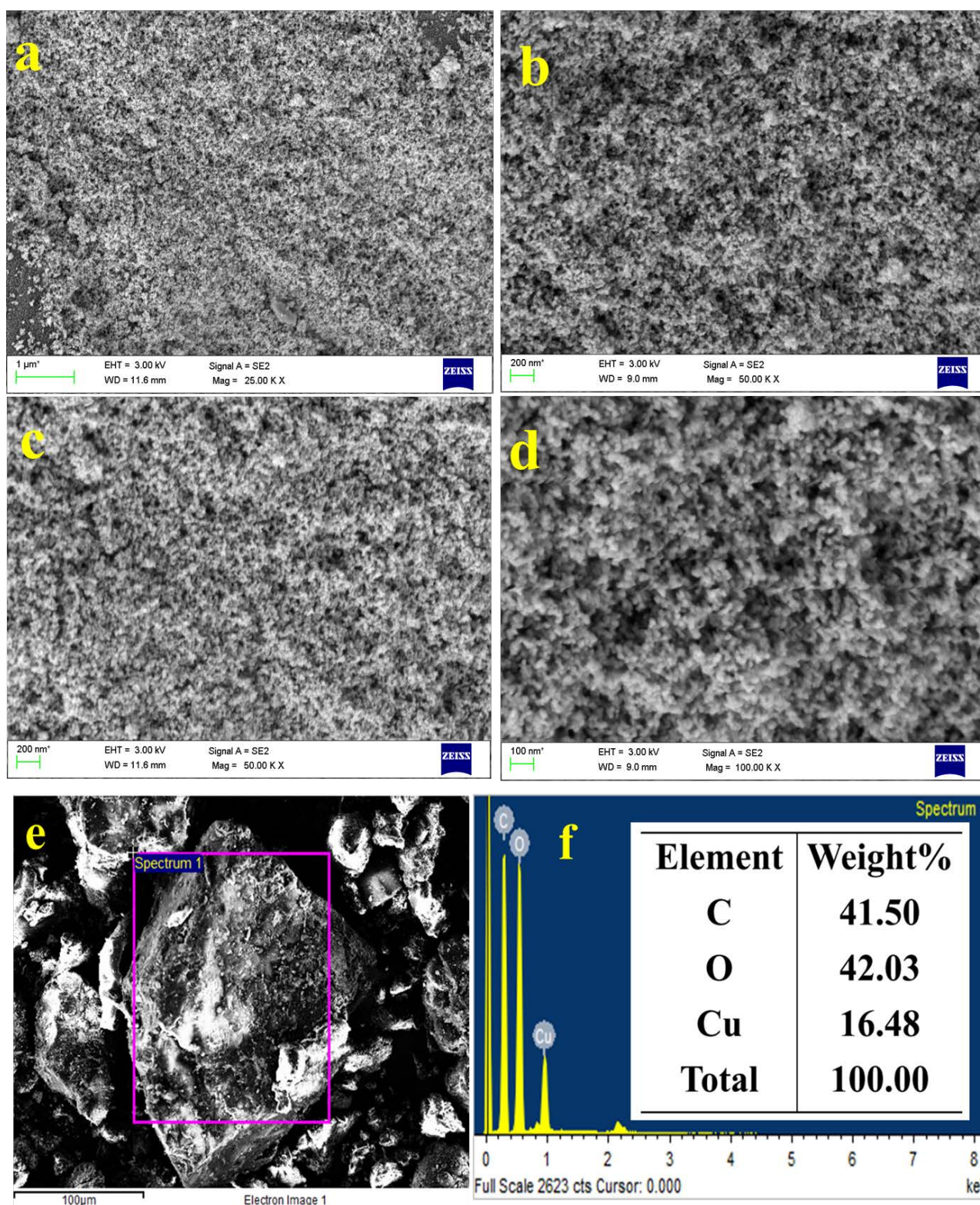


Figure 10. SEM micrographs (a–d) EDS spot (e) and EDS spectra (f) of CuONPs synthesized by *A. saman*.

4.8. Morphological Analysis of CuONPs Using TEM

Figure 11a–c shows the TEM images of the CuONPs synthesized from *A. saman* at different nm scales. Figure 11a shows roughly spherical-shaped CuONPs at 200 nm scale. The dark spots are Cu-rich regions, while the bright spots are organic carbon-rich regions,

indicating the association of carbon compounds with the synthesized CuONPs. Figure 11b also shows roughly spherical-shaped CuONPs along with aggregation. Figure 11c shows the CuONPs at 50 nm scale, where the particles are clearly visible in their almost spherical shape. Moreover, the particles are also showing aggregation, which is revealed by the TEM images. The size of the individual roughly spherical CuONPs is 20–50 nm. Figure 11d shows the scattering area electron diffraction pattern of the CuONPs synthesized from *A. saman* at a 10 nm scale, where the sharp spots in a ring pattern show the polycrystalline nature of the phytonanofabricated CuO. Earlier, a team led by Jayakumarai utilized the leaf extract of *A. lebbbeck* and synthesized CuONPs of a size below 100 nm [64].

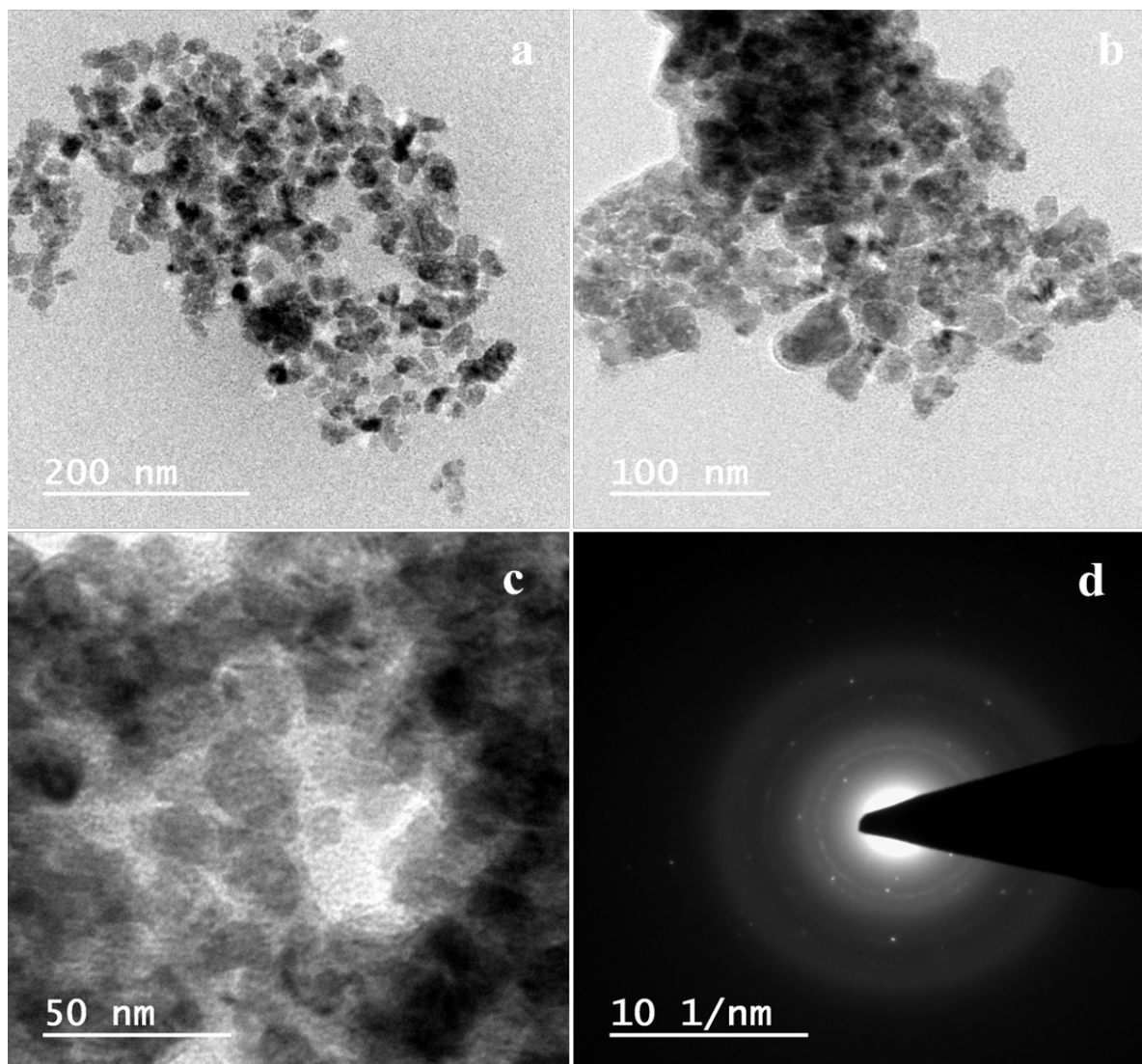


Figure 11. TEM micrographs (a–c) and SAED pattern (d) of CuONPs.

4.9. Adsorption Results of Congo Red Using CuONPs

The adsorption capacity of phytofabricated CuONPs was evaluated by measuring the leftover concentration of dye in an aqueous medium using a UV-Vis spectrophotometer [71]. The CR dye showed a maximum absorption peak (λ_{\max}) at 498 nm. The concentration of dye was measured up to 1 h at regular intervals of 5 min. Figure 12a shows the CR adsorption spectrum, and based on this spectrum effect of contact time, a kinetic study for the adsorption of CR dye was conducted.

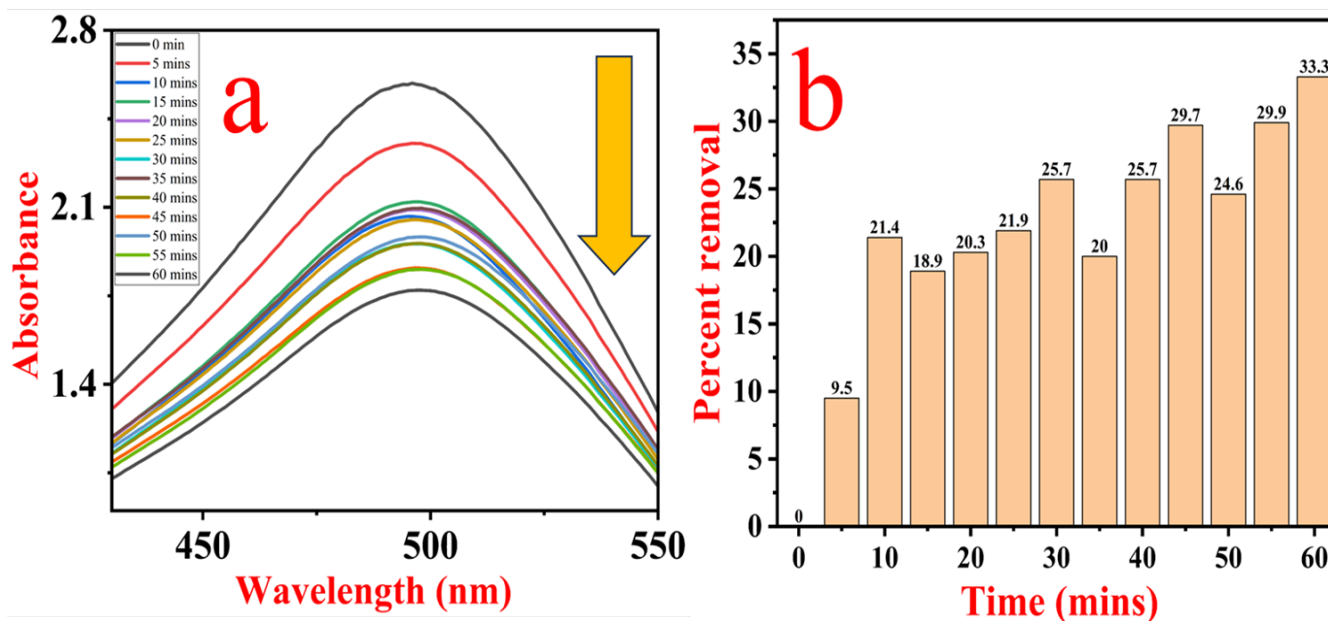


Figure 12. Absorption spectrum of Congo Red dye (a) and removal percentage of CR dye (b) CuONPs.

The remediation of CR from its aqueous medium takes place either via physisorption, chemisorption method, or photocatalytic degradation. The adsorption of CR onto the surface of CuONPs continuously increased up to 60 min. The percent removal [72] of CR using a fixed amount of adsorbent for up to 60 min is shown in Figure 12b.

Figure 13b,c shows that CR removal efficiency was enhanced with time, whereas the percent remediation of CR decreased with the increase in CR concentration. After 60 min, the removal percentage of CR was 33.3% for 50 ppm. The results obtained here were in close agreement with the previous results reported by Swathilakshmi and colleagues for CR dye adsorption by CuONPs [63]. The adsorption capacity of CuONPs varied from 5 to 17.53 mg/g against the adsorption of CR dye. The pseudo-first-order kinetics (Figure 13b) and pseudo-second-order kinetics (Figure 13c) were performed and their values are given below in Table 3.

Table 3. Kinetics study of CuONPs for adsorption of CR dye.

Co (mg/L)	qe (mg/g)	PFO		PSO	
		K1 (min ⁻¹)	R ²	K2 (min ⁻¹)	R ²
50	16	−0.2142	0.6927	0.0642	0.8995

Earlier, Batool obtained the highest removal for CR dye in 120 min, i.e., 1.1 mg/g from the 80 to 120 nm sized CuONPs synthesized from *Aloe vera* [73]. Jethave and colleagues also synthesized CuONPs from the *Nyctanthes arbortristis* leaf extract and removed CR dye from aqueous solution. The kinetic study revealed that the CR dye adsorption on CuONPs followed PFO reactions. Langmuir isotherm modeling was found to be best fitted and describes the CR dye adsorption by CuONPs in 1 hour 30 min with Q_{max} at 333.33 (mg/g) [74]. Rasheed and colleagues obtained a photocatalytic degradation of about 94% with Cu₂O and 54% with CuONPs for the remediation of CR dye [75]. Zahrah Alhalili (2022) synthesized spherical-shaped CuONPs of an average size of 88 nm from the leaf extract of *E. golobulus*. The nano adsorbent remediated the methyl orange dye up to 95 mg/g from the aqueous solution [59]. Venkata and colleagues used CuONPs synthesized from *S. nigrum* for the efficient removal of CR with 64.448 ± 1.141%, Coomassie Brilliant Blue R-250 (CBB) 75.302 ± 2.072%, and Methylene Blue 89.339 ± 0.739%. Table 4 shows a comparison of CR dye remediation from aqueous solution using different adsorbents.

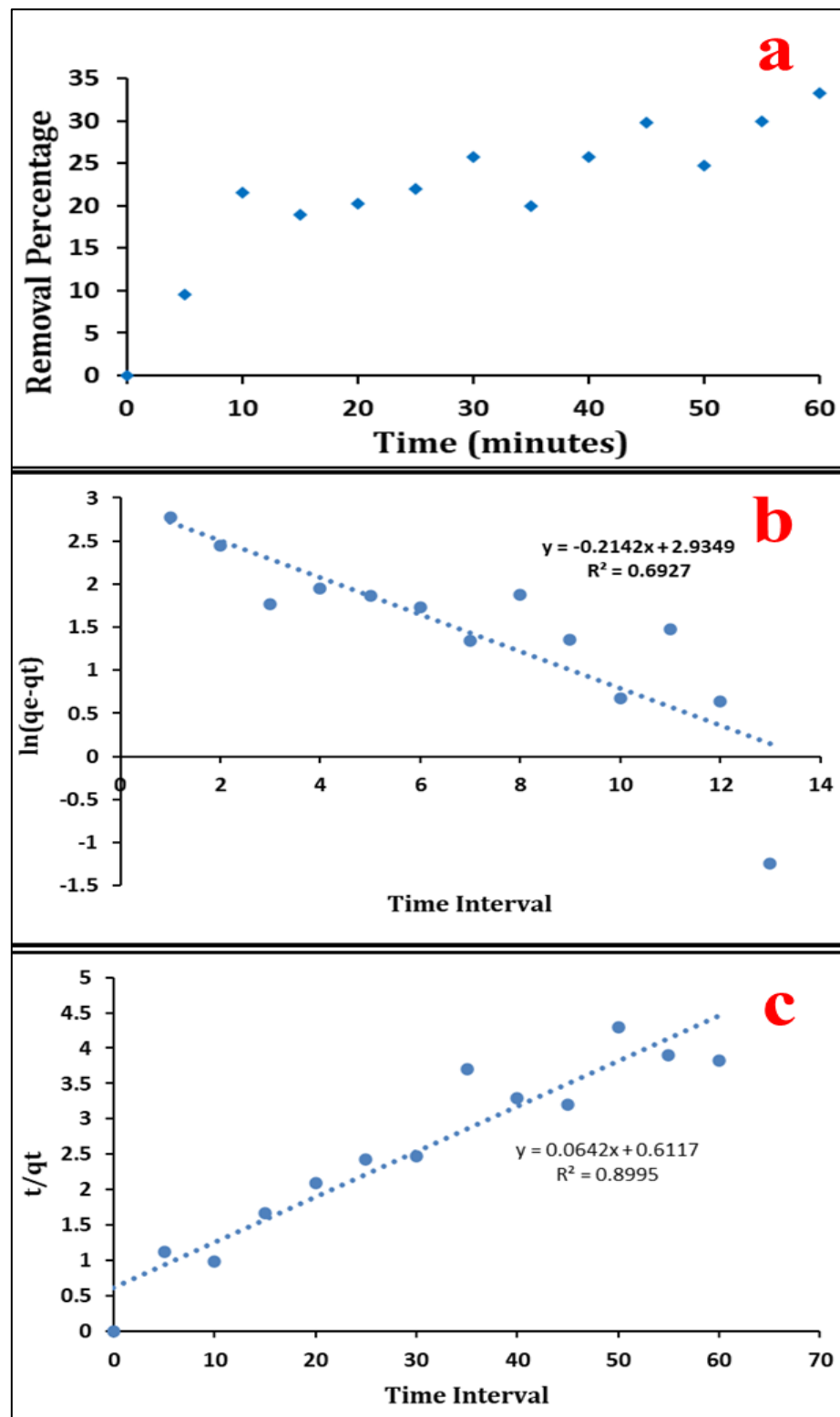


Figure 13. (a) Graph representing contact time v/s adsorption capacity of CuONPs, (b) pseudo-first-order kinetics and (c) pseudo-second-order kinetics.

Table 4. A comparative investigation of the remediation of CR dye from aqueous solution utilizing various adsorbents.

Adsorbent	Dose of Adsorbent (g/L)	Removal Efficiency	Adsorption Capacity (mg/g)	Temp	Contact Time (Minutes)	References
Coal fly ash	1		13.5			[76]
	2.5		9			
	4		6			
CuONPs	5 mg/g		1.1		10	[73]
CuONPs	10 mg/L	100%			35	[77]
	60 mg/L	100%			2	
ZnONPs	0.05 g	95.5%			20	[78]
IONPs from incense stick ash	10 mg/L	72%		30 °C	60	[44]
Groundnut shell charcoal	100 mg in 100 mL	80%	117.6	318 K		[79]
Eichhornia charcoal (EC)	100 mg in 100 mL	60%	56.8	318 K		
Pine bark	1–10 g L ⁻¹	23.4 to 100%	0.3 to 1.6 mg·g ⁻¹	25–60 °C	0–7 days	[80]
<i>Moringa oleifera</i> seed coat		>90%		321 K	90 min	[81]
CuONPs		33.3%	17.53 mg/g			Current investigation

From the above table, it can be seen that the dye removal percentage depends on several factors, like temperature and Ph, the dose of adsorbent, contact time, and the morphology of the adsorbent. A study led by Kaur showed that increasing the temperature by a few degrees may drastically increase Congo Red dye removal efficiency using groundnut shell charcoal and EC [79].

4.10. Mechanism of Congo Red Dye Removal by CuONPs

Copper oxide exhibits photocatalytic properties in sunlight and UV light, which remediates the colored dye much more efficiently. The removal percentage of color dye from wastewater or aqueous solution depends on the size of the CuONPs and the charge on the synthesized CuONPs. Figure 14 shows the probable mechanism of removal of CR dye from aqueous solution using CuONPs. When the dye is removed in open conditions in the laboratory, the CuONPs simply act as an adsorbent that adsorbs the dye molecules through various interactions, like Vander Wall forces, electrostatic interaction, etc. [82]. Moreover, the CuONPs have various charged functional groups, which attract or repel the dye molecules and remove the dye from the medium. In the presence of sunlight, electron from the valence band (VB) of CuONPs excites and reaches the conduction band (CB), which leads to the formation of an electron–hole pair. These holes in the BV react with the OH group on the surface of the CuONPs and reduce them to more reactive [OH·]. Further, the e⁻s in the CB react with O₂ molecules adsorbed on the surface of the CuONPs, which are being oxidized into superoxide anion radicals [O₂·]. The developed highly reactive free radicals interact with the CR dye molecules, which results in the generation of CO₂, H₂O, and other by-products through oxidative decomposition. A similar mechanism has also been elucidated by Venkata and colleagues via CuONPs synthesized from the leaf extract of *S. nigrum* under sunlight [83]. A team led by Kumar also showed a similar kind of mechanism for the remediation of organic pollutants and heavy metals from wastewater using a porous boron nitride-magnetic hydrogel [84].

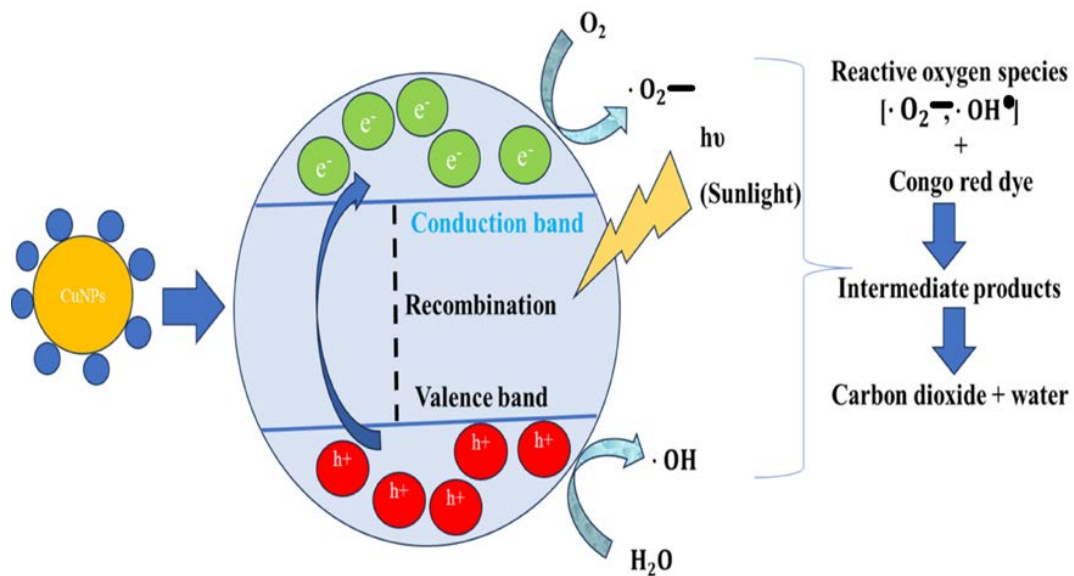


Figure 14. Probable mechanism of CR dye degradation using CuONPs synthesized from *A. saman* [83].

4.11. Regeneration Study of CuONPs

The regeneration study of the adsorbent was conducted by collecting the adsorbent after the 1st cycle, followed by washing with distilled water and ethanol. Further, the CuONPs were dried overnight in an oven at 50 °C. The dried CuONPs were then reused for the removal of 50 ppm CR dye from aqueous solution. An aliquot was taken after 60 min of contact time, which was analyzed using a UV-Vis instrument to detect the conc. A similar step was also performed for cycles 3 and 4. All other conditions were almost the same in all the cycles, like temperature, conc of CR dye, stirring speed, and contact time. After the first cycle, the removal percentage of CR dye was about 33.5% at 60 min for 50 ppm CR dye, which was further reduced to 25.6% after the 2nd cycle, 19.3% after the 3rd cycle, and 16% after the 4th cycle. Said and colleagues also conducted a reusability test of CuONPs synthesized via the chemical route. The removal efficiency for the first cycle was almost 100%, which decreased to 98% after the second cycle, 97% after the 3rd cycle, and 95% after the 4th cycle [77], as shown in Figure 15.

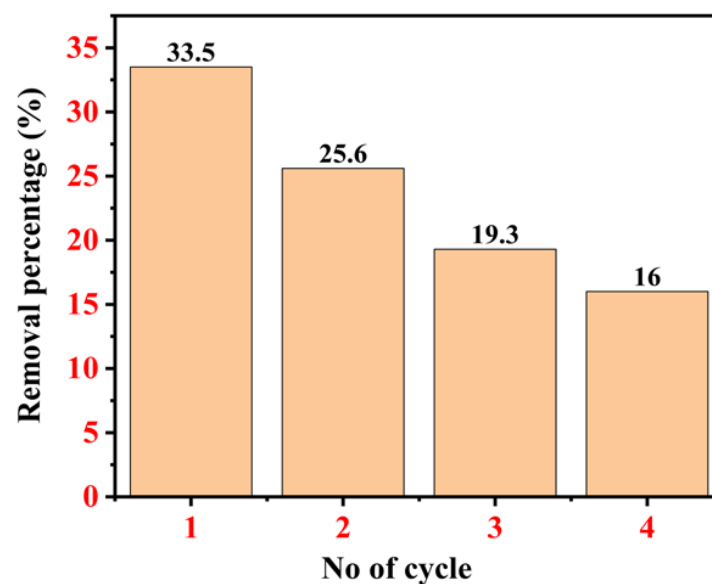


Figure 15. Recyclability test of CuONPs synthesized from *A. saman* obtained from ethanol after elimination of CR dye.

4.12. Antimicrobial Activity of CuONPs

The antimicrobial activity of CuONPs was evaluated by calculating the ZOI technique against *E. coli* [Gram-negative (GN)] and *S. aureus* [Gram-positive (GP)] bacteria and *C. albicans* yeast. An aqueous solution of 1 mg per 3 mL of ddw was found effective against all the microbial strains and exhibited antimicrobial activity. The antimicrobial activity revealed a ZOI of about 15 mm against *E. coli*, whereas the ZOI against *S. aureus* was about 14 mm. So, the phytonanofabricated CuO particles were found to be more effective against GN *E. coli* than GP *S. aureus*. CuONPs, being smaller in size, may easily gain access to the bacteria and inhibit the enzyme activity, thereby affecting the major metabolic functions. Moreover, Cu is a heavy metal that reacts with the sulfhydryl groups of the enzyme and inhibits their growth. Furthermore, being GN, *E. coli* has a thin layer of peptidoglycan compared with the GP *S. aureus*. Therefore, there might be more entry of CuONPs into the *E. coli*, inhibiting their growth. The antimicrobial activity of CuONPs of the same concentration was evaluated against *C. Albicans* and showed a ZOI of 12 mm (Figure 16).

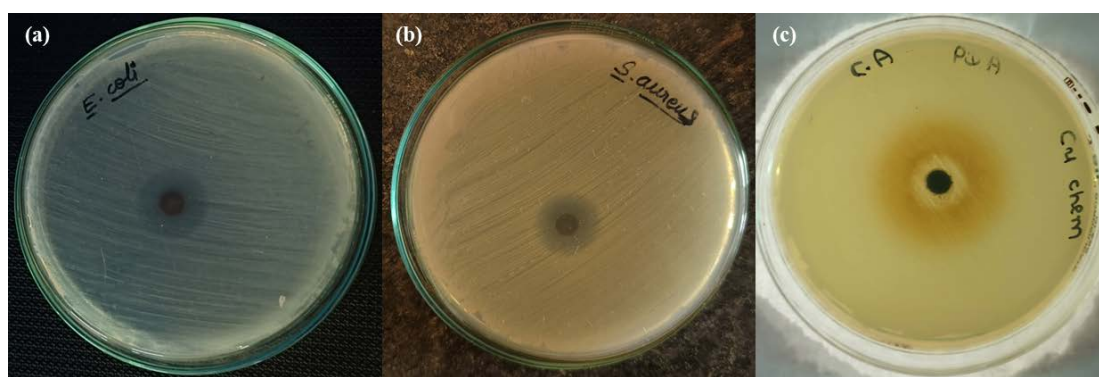


Figure 16. Antimicrobial activity of CuONPs against (a) *E. coli*, (b) *S. aureus*, and (c) *C. albicans*.

Earlier, a team led by Singh also observed the antimicrobial effect of 500 and 1000 μg of CuONPs synthesized from the plant extract of *Annona squamosa*. The investigators obtained a ZOI of about 21 mm against *E. coli* and 17 mm against *Microbacterium testaceum* at a concentration of 1000 μg . The investigators also obtained a higher ZOI against GN *E. coli* in comparison with GP *M. testaceum*. Moreover, the investigators suggested that the antimicrobial effect of the phytonanofabricated CuONPs could be due to their interaction with the bacterial plasma membrane, which leads to the formation of holes in the membrane, and ultimately, cell lysis. Furthermore, it was observed that the Cu^{2+} ions interact with the bacterial components of the cell wall, resulting in a negative charge, which causes the denaturation and alteration of membranous proteins. In addition to this, once the Cu^{2+} ions reach the inside of the bacterial cell, they produce ROS, which leads to alterations in the cellular signaling and interference with the nucleic acid. This ultimately results in altered helical morphology [85]. A group led by Chen synthesized 40–80 nm sized CuONPs from papaya leaf extracts and evaluated their antimicrobial activity against the soil-borne pathogen, *Rolstonia solanacearum*. The investigators obtained a reduction of about 35–37% in the growth of *R. solanacearum*, whose optical density was measured at 600 nm wavelength [86]. Nabila and Kannabiran (2018) synthesized 61.7 nm sized CuONPs and assessed their antimicrobial property against several fish pathogenic bacteria, out of which *Bacillus cereus* was found to be the most susceptible, i.e., 25.3 mm (ZOI) [87]. Table 5 shows a comparative study of the antimicrobial properties of CuONPs.

Table 5. A comparative study of the antimicrobial properties of CuONPs synthesized from plants.

Plant Used	Tested Microorganism	ZOI (mm)	Method Used	References
<i>Annona squamosa</i>	<i>Microbacterium testaceum</i>	17	Agar-well diffusion	[85]
	<i>E. coli</i>	21		
<i>Silybum marianum</i> (leaf extract)	<i>Enterobacter aerogenes</i>	18 ± 1.3		[88]
	<i>Salmonella typhi</i>	17 ± 1.2		
	<i>Bacillus cereus</i>	225.3		
<i>Aerva javanica</i> (at 100 µg/mL): leaf extract	<i>E. coli</i>	6 ± 1	Agar-well diffusion	[89]
	<i>Acinetobacter baumannii</i>	12 ± 1		
	<i>S. aureus</i>	12 ± 1		
	<i>Pseudomonas aeruginosa</i>	10 ± 1		
	<i>C. albicans</i>	9 + 0.5		
	<i>C. albicans</i>	7 + 1		
	<i>C. krusei</i>	5 + 1		
	<i>C. tropicalis</i>	4 + 0		
<i>A. javanica</i> (at 200 µg/mL): leaf extract	<i>E. coli</i>	7 ± 0.57		
	<i>A. baumannii</i>	12 ± 1		
	<i>S. aureus</i>	12 ± 1		
	<i>P. aeruginosa</i>	13 ± 1		
<i>Berberis vulgaris</i> (leaf extract)	<i>S. aureus</i> ATCC 29213	MIC (µg/mL): 0.3 MBC (µg/mL): 2.4	Tube dilution method	[90]
	<i>K. pneumoniae</i> ATCC 700603	MIC (µg/mL): 1.2 MBC (µg/mL): 4.8		
	<i>E. coli</i> ATCC 25922	MIC (µg/mL): 0.6 MBC (µg/mL): 2.4		
<i>Silybum marianum</i> (Leaf extract) 4 mg mL ⁻¹	<i>Micrococcus luteus</i>	5 ± 0.8		
	<i>Salmonella typhi</i>	9 ± 1.1		
	<i>Salmonella setubal</i>	8 ± 0.9		
	<i>S. aureus</i>	4 ± 0.6		
	<i>E. aerogenes</i>	9 ± 0.9		
<i>S. marianum</i> (Leaf extract) 20 mg mL ⁻¹	<i>M. luteus</i>	8 ± 0.7	Agar-disc diffusion	[88]
	<i>S. typhi</i>	17 ± 1.2		
	<i>S. setubal</i>	16 ± 1.2		
	<i>S. aureus</i>	7 ± 0.7		
	<i>E. aerogenes</i>	18 ± 1.3		
<i>Albizia saman</i> (leaf extract)	<i>E. coli</i>	15	Agar-well diffusion	Current investigation
	<i>S. aureus</i>	14		
	<i>C. albicans</i>	12		

From the above table, it could be concluded that the dose of CuONPs may exert a positive effect on antimicrobial activity, i.e., at higher doses, there is more interaction with the pathogenic microorganisms, leading to their greater inhibition, and ultimately, a higher ZOI [89]. However, in a study, higher concentrations of CuONPs, i.e., 20 mg/mL, exhibited a higher bactericidal effect of the CuONPs compared with the 4 mg/mL concentration. The inhibitory effect might be due to the interaction of the external bacterial membrane with the CuONPs. These CuONPs may disrupt the integrity of the membrane of the bacteria, which may further cause malfunctioning of enzymes and enhanced cell permeability, leading to the death of the bacteria. Moreover, the integration of the CuONPs inside the cell membrane might be due to the smaller size of the pores on the bacterial cell membrane [88].

4.13. Mechanism of Antimicrobial Activity of CuONPs

The Cu itself is considered a heavy metal that reacts with the proteins and enzymes of microbes and inhibits their growth. The nanosized CuO easily enters microbes and affects the internal organelles of the microorganism (mainly bacteria), resulting in damage, and ultimately, death of the microorganisms. The exact mode of action of CuONPs as an antimicrobial agent is not yet clear, but it is considered that there might be a release of ionic Cu from the metallic Cu surfaces. Secondly, there could be leaching of copper ions from CuONPs. Thirdly, there might be the production of reactive oxygen species (ROS), which may irreversibly damage membranes. Previously, a study demonstrated that the antibacterial activity of CuONPs is due to the release of Cu^{2+} . Due to the very small size of the Cu^{2+} , it could easily gain access through the bacteria cell membranes, thereby disrupting the functions of the enzyme. Moreover, there is an indirect effect through changes in the surrounding charge environment of microorganisms [91,92].

5. Conclusions

The roughly spherical-shaped CuONPs of 20–50 nm was successfully synthesized using methanolic leaf extracts of *A. saman*. The methanolic extracts of the *A. saman* leaf have flavonoids, tannins, terpenoids, and several other biomolecules. These phytochemical acts as major capping and reducing agents during the formation of CuONPs. The phytonanofabricated CuO particles were analyzed to determine their detailed properties using analytical instruments. The FTIR revealed the band at 530 cm^{-1} , which was attributed to Cu-O. The FTIR and FESEM showed the association of organic molecules with the developed CuONPs. The average size of the crystalline CuONPs was 29 nm. The CR adsorption study showed that 33.3% remediation of the dye compound from its aqueous solution was achieved, whereas the highest adsorption capacity of CuONPs was measured as 17.53 mg/g against adsorption of 50 ppm of CR dye. The removal efficiency of CR dye by the phytonanofabricated CuO was reduced to almost half after the 4th cycle.

Author Contributions: Conceptualization, N.C., J.C., V.M. and P.P.; Methodology, N.C., P.P., J.C., V.M., D.A. and S.A.; Software, D.A., S.A., D.K.S. and V.K.Y.; Validation, P.P., D.A., D.K.S. and A.P.; Formal analysis, J.C., V.M. and D.K.S.; Investigation, V.K.Y., S.A. and A.P.; Resources, D.A., S.A., D.K.S. and A.P.; Writing—original draft, N.C., V.M., P.P., J.C. and V.K.Y.; Writing—review & editing, A.P., D.A., S.A., D.K.S. and A.P.; Supervision, N.C., V.K.Y. and A.P.; Project administration, N.C., V.K.Y. and A.P.; Funding acquisition, D.A. and S.A. All authors have read and agreed to the published version of the manuscript.

Funding: This research received no external funding.

Data Availability Statement: Data will be made available on request.

Acknowledgments: This research was supported by the Researchers Supporting Project number (RSP2023R27), King Saud University, Riyadh, Saudi Arabia. The authors are grateful to the Department of Life Sciences for providing laboratory facilities and infrastructure.

Conflicts of Interest: The authors declare no competing financial interest.

References

1. Nisha, C.; Bhawana, P.; Fulekar, M.H. Antimicrobial Potential of Green Synthesized Silver Nanoparticles Using *Sida Acuta* Leaf Extract. *Nano Sci. Nano Technol.* **2017**, *11*, 111–119.
2. Shen, Q.; Lu, Z.; Bi, F.; Zhang, D.; Li, L.; Zhang, X.; Yang, Y.; Wu, M. Regulating Electronic Metal-Support Interaction by Synthetic Methods to Enhance the Toluene Degradation over Pt/Co₃O₄ Catalysts. *Sep. Purif. Technol.* **2023**, *325*, 124707. [[CrossRef](#)]
3. Bi, F.; Ma, S.; Gao, B.; Liu, B.; Huang, Y.; Qiao, R.; Zhang, X. Boosting Toluene Deep Oxidation by Tuning Metal-Support Interaction in MOF-Derived Pd@ZrO₂ Catalysts: The Role of Interfacial Interaction between Pd and ZrO₂. *Fuel* **2024**, *357*, 129833. [[CrossRef](#)]
4. Dadhwal, P.; Dhingra, H.K.; Dwivedi, V.; Alarifi, S.; Kalasariya, H.; Yadav, V.K.; Patel, A. *Hippophae Rhamnoides*, L. (Sea Buckthorn) Mediated Green Synthesis of Copper Nanoparticles and Their Application in Anticancer Activity. *Front. Mol. Biosci.* **2023**, *10*, 1246728. [[CrossRef](#)]
5. Yadav, V.K.; Amari, A.; Gacem, A.; Elboughdiri, N.; Eltayeb, L.B.; Fulekar, M.H. Treatment of Fly-Ash-Contaminated Wastewater Loaded with Heavy Metals by Using Fly-Ash-Synthesized Iron Oxide Nanoparticles. *Water* **2023**, *15*, 908. [[CrossRef](#)]
6. Ocheje Ameh, P. Synthesized Iron Oxide Nanoparticles from *Acacia Nilotica* Leaves for the Sequestration of Some Heavy Metal Ions in Aqueous Solutions. *J. Chem. Lett.* **2023**, *4*, 38–51. [[CrossRef](#)]
7. Trinh, T.T.P.N.X.; Trinh, D.N.; Cuong, D.C.; Hai, N.D.; Huong, L.M.; Thinh, D.B.; Hoa, H.N.; Cong, C.Q.; Nam, N.T.H.; An, H.; et al. Optimization of Crystal Violet Photodegradation and Investigation of the Antibacterial Performance by Silver-Doped Titanium Dioxide/Graphene Aerogel Nanocomposite. *Ceram. Int.* **2023**, *49*, 20234–20250. [[CrossRef](#)]
8. Choudhary, N.; Yadav, V.K.; Ali, H.; Ali, D.; Almutairi, B.O.; Cavalu, S.; Patel, A. Remediation of Methylene Blue Dye from Wastewater by Using Zinc Oxide Nanoparticles Loaded on Nanoclay. *Water* **2023**, *15*, 1427. [[CrossRef](#)]
9. Fouda, A.; Saied, E.; Eid, A.M.; Kouadri, F.; Alemam, A.M.; Hamza, M.F.; Alharbi, M.; Elkelish, A.; Hassan, S.E.D. Green Synthesis of Zinc Oxide Nanoparticles Using an Aqueous Extract of *Punica Granatum* for Antimicrobial and Catalytic Activity. *J. Funct. Biomater.* **2023**, *14*, 205. [[CrossRef](#)]
10. Tijani, J.O.; Odeh, E.L.; Mustapha, S.; Egbosiuba, T.C.; Daniel, A.I.; Abdulkareem, A.S.; Muya, F.N. Photocatalytic, Electrochemical, Antibacterial and Antioxidant Behaviour of Carbon-Sulphur Co-Doped Zirconium (IV) Oxide Nanocomposite. *Clean. Chem. Eng.* **2022**, *3*, 100034. [[CrossRef](#)]
11. Wang, Y.; Yang, L.; Xu, J.; Xin, F.; Jiang, L. Applications of Synthetic Microbial Consortia in Biological Control of Mycotoxins and Fungi. *Curr. Opin. Food Sci.* **2023**, *53*, 101074. [[CrossRef](#)]
12. Yadav, V.K.; Amari, A.; Wanale, S.G.; Osman, H.; Fulekar, M.H. Synthesis of Floral-Shaped Nanosilica from Coal Fly Ash and Its Application for the Remediation of Heavy Metals from Fly Ash Aqueous Solutions. *Sustainability* **2023**, *15*, 2612. [[CrossRef](#)]
13. Modi, S.; Yadav, V.K.; Amari, A.; Alyami, A.Y.; Gacem, A.; Harharah, H.N.; Fulekar, M.H. Photocatalytic Degradation of Methylene Blue Dye from Wastewater by Using Doped Zinc Oxide Nanoparticles. *Water* **2023**, *15*, 2275. [[CrossRef](#)]
14. Chahar, M.; Khaturia, S.; Singh, H.L.; Solanki, V.S.; Agarwal, N.; Sahoo, D.K.; Yadav, V.K.; Patel, A. Recent Advances in the Effective Removal of Hazardous Pollutants from Wastewater by Using Nanomaterials—A Review. *Front. Environ. Sci.* **2023**, *11*, 1226101. [[CrossRef](#)]
15. Dizaj, S.M.; Lotfipour, F.; Barzegar-Jalali, M.; Zarrintan, M.H.; Adibkia, K. Antimicrobial Activity of the Metals and Metal Oxide Nanoparticles. *Mater. Sci. Eng. C* **2014**, *44*, 278–284. [[CrossRef](#)]
16. Kotrange, H.; Najda, A.; Bains, A.; Gruszecki, R.; Chawla, P.; Tosif, M.M.; Thakur, K. Molecular Sciences Metal and Metal Oxide Nanoparticle as a Novel Antibiotic Carrier for the Direct Delivery of Antibiotics. *J. Mol. Sci.* **2021**, *22*, 9596. [[CrossRef](#)] [[PubMed](#)]
17. Gobane, S.; Dama, T.; Hasan, N.; Yanmaz, E. Characterization of Copper Oxide-Jatropha Oil Nanofluid as a Secondary Refrigerant. *J. Nanomater.* **2023**, *2023*, 7612959. [[CrossRef](#)]
18. Baig, U.; Ansari, M.A.; Gondal, M.A.; Akhtar, S.; Khan, F.A.; Falath, W.S. Single Step Production of High-Purity Copper Oxide-Titanium Dioxide Nanocomposites and Their Effective Antibacterial and Anti-Biofilm Activity against Drug-Resistant Bacteria. *Mater. Sci. Eng. C* **2020**, *113*, 110992. [[CrossRef](#)] [[PubMed](#)]
19. Emima Jeronsia, J.; Allwin Joseph, L.; Annie Vinosha, P.; Jerline Mary, A.; Jerome Das, S. *Camellia Sinensis* Leaf Extract Mediated Synthesis of Copper Oxide Nanostructures for Potential Biomedical Applications. *Mater. Today Proc.* **2019**, *8*, 214–222. [[CrossRef](#)]
20. Halbus, A.F.; Horozov, T.S.; Paunov, V.N. Strongly Enhanced Antibacterial Action of Copper Oxide Nanoparticles with Boronic Acid Surface Functionality. *ACS Appl. Mater. Interfaces* **2019**, *11*, 12232–12243. [[CrossRef](#)]
21. Guo, Z.; Zhan, R.; Shi, Y.; Zhu, D.; Pan, J.; Yang, C.; Wang, Y.; Wang, J. Innovative and Green Utilization of Zinc-Bearing Dust by Hydrogen Reduction: Recovery of Zinc and Lead, and Synergetic Preparation of Fe/C Micro-Electrolysis Materials. *Chem. Eng. J.* **2023**, *456*, 141157. [[CrossRef](#)]
22. Waris, A.; Din, M.; Ali, A.; Ali, M.; Afridi, S.; Baset, A.; Ullah Khan, A. A Comprehensive Review of Green Synthesis of Copper Oxide Nanoparticles and Their Diverse Biomedical Applications. *Inorg. Chem. Commun.* **2021**, *123*, 108369. [[CrossRef](#)]
23. Nagajyothi, P.C.; Muthuraman, P.; Sreekanth, T.V.M.; Kim, D.H.; Shim, J. Green Synthesis: In-Vitro Anticancer Activity of Copper Oxide Nanoparticles against Human Cervical Carcinoma Cells. *Arab. J. Chem.* **2017**, *10*, 215–225. [[CrossRef](#)]
24. Vishnu, S.; Ramaswamy, P.; Narendhran, S.; Sivaraj, R. Potentiating Effect of Ecofriendly Synthesis of Copper Oxide Nanoparticles Using Brown Alga: Antimicrobial and Anticancer Activities. *Bull. Mater. Sci.* **2016**, *39*, 361–364.

25. Ramírez, A.E.; Montero-Muñoz, M.; López, L.L.; Ramos-Ibarra, J.E.; Coaquira, J.A.H.; Heinrichs, B.; Páez, C.A. Significantly Enhancement of Sunlight Photocatalytic Performance of ZnO by Doping with Transition Metal Oxides. *Sci. Rep.* **2021**, *11*, 2804. [[CrossRef](#)] [[PubMed](#)]
26. Akintelu, S.A.; Folorunso, A.S.; Folorunso, F.A.; Oyebamiji, A.K. Green Synthesis of Copper Oxide Nanoparticles for Biomedical Application and Environmental Remediation. *Heliyon* **2020**, *6*, e04508. [[CrossRef](#)]
27. Ahmed, F.; Javed, B.; Razzaq, A.; Mashwani, Z.-R. Applications of Copper and Silver Nanoparticles on Wheat Plants to Induce Drought Tolerance and Increase Yield. *IET Nanobiotechnol.* **2021**, *15*, 68–78. [[CrossRef](#)]
28. Wang, Z.; Chen, C.; Liu, H.; Hrynsphan, D.; Savitskaya, T.; Chen, J.; Chen, J. Enhanced Denitrification Performance of *Alcaligenes* Sp. TB by Pd Stimulating to Produce Membrane Adaptation Mechanism Coupled with Nanoscale Zero-Valent Iron. *Sci. Total Environ.* **2020**, *708*, 135063. [[CrossRef](#)] [[PubMed](#)]
29. Sun, S.J.; Deng, P.; Peng, C.E.; Ji, H.Y.; Mao, L.F.; Peng, L.Z. Extraction, Structure and Immunoregulatory Activity of Low Molecular Weight Polysaccharide from *Dendrobium Officinale*. *Polymers* **2022**, *14*, 2899. [[CrossRef](#)]
30. Rahman, I.A.; Padavettan, V. Synthesis of Silica Nanoparticles by Sol-Gel: Size-Dependent Properties, Surface Modification, and Applications in Silica-Polymer Nanocomposites: A Review. *J. Nanomater.* **2012**, *2012*, 132424. [[CrossRef](#)]
31. Dong, Y.; Yuan, H.; Ge, D.; Zhu, N. A Novel Conditioning Approach for Amelioration of Sludge Dewaterability Using Activated Carbon Strengthening Electrochemical Oxidation and Realized Mechanism. *Water Res.* **2022**, *220*, 118704. [[CrossRef](#)]
32. Wang, Z.; Hu, L.; Zhao, M.; Dai, L.; Hrynsphan, D.; Tatsiana, S.; Chen, J. Bamboo Charcoal Fused with Polyurethane Foam for Efficiently Removing Organic Solvents from Wastewater: Experimental and Simulation. *Biochar* **2022**, *4*, 28. [[CrossRef](#)]
33. Chukwu Onu, D.; Kamoru Babayemi, A.; Chinedu Egbojiuba, T.; Onyinye Okafor, B.; Jacinta Ani, I.; Mustapha, S.; Oladejo Tijani, J.; Chukwuemeke Ulakpa, W.; Eguono Ovuoraye, P.; Saka Abdulkareem, A. Isotherm, Kinetics, Thermodynamics, Recyclability and Mechanism of Ultrasonic Assisted Adsorption of Methylene Blue and Lead (II) Ions Using Green Synthesized Nickel Oxide Nanoparticles. *Environ. Nanotechnol. Monit. Manag.* **2023**, *20*, 100818. [[CrossRef](#)]
34. Shah, N.; Nisar, N.; Rehan, T.; Naeem, M.; Ul-Islam, M. Microwave-Assisted Synthesis of a Magnetic Core-Shell Material Composed of Fe₃O₄@SiO₂@poly(Methacrylamide-Co-Acrylic Acid) for an Anticancer Drug Loading. *Appl. Nanosci.* **2022**, *12*, 3547–3554. [[CrossRef](#)]
35. Singh, J.; Dutta, T.; Kim, K.-H.; Rawat, M.; Samddar, P.; Kumar, P. 'Green' Synthesis of Metals and Their Oxide Nanoparticles: Applications for Environmental Remediation. *J. Nanobiotechnol.* **2018**, *16*, 84. [[CrossRef](#)] [[PubMed](#)]
36. Nikolova, M.P.; Joshi, P.B.; Chavali, M.S. Updates on Biogenic Metallic and Metal Oxide Nanoparticles: Therapy, Drug Delivery and Cytotoxicity. *Pharmaceutics* **2023**, *15*, 1650. [[CrossRef](#)] [[PubMed](#)]
37. Chen, D.; Wang, Q.; Li, Y.; Li, Y.; Zhou, H.; Fan, Y. A General Linear Free Energy Relationship for Predicting Partition Coefficients of Neutral Organic Compounds. *Chemosphere* **2020**, *247*, 125869. [[CrossRef](#)] [[PubMed](#)]
38. Letchumanan, D.; Sok, S.P.M.; Ibrahim, S.; Nagoor, N.H.; Arshad, N.M. Plant-Based Biosynthesis of Copper/Copper Oxide Nanoparticles: An Update on Their Applications in Biomedicine, Mechanisms, and Toxicity. *Biomolecules* **2021**, *11*, 564. [[CrossRef](#)]
39. Yu, M.; Gouvinhas, I.; Rocha, J.; Barros, A.I.R.N.A. Phytochemical and Antioxidant Analysis of Medicinal and Food Plants towards Bioactive Food and Pharmaceutical Resources. *Sci. Rep.* **2021**, *11*, 10041. [[CrossRef](#)]
40. Cao, Y.; Dhahad, H.A.; El-Shorbagy, M.A.; Alijani, H.Q.; Zakeri, M.; Heydari, A.; Bahonar, E.; Slouf, M.; Khatami, M.; Naderifar, M.; et al. Green Synthesis of Bimetallic ZnO–CuO Nanoparticles and Their Cytotoxicity Properties. *Sci. Rep.* **2021**, *11*, 23479. [[CrossRef](#)]
41. Daphedar, A.; Taranath, T.C. Biosynthesis of Silver Nanoparticles by Leaf Extract of *Albizia Saman* (Jacq.) Merr. and Their Cytotoxic Effect on Mitotic Chromosomes of *Drimia Indica* (Roxb.) Jessop. *Environ. Sci. Pollut. Res.* **2017**, *24*, 25861–25869. [[CrossRef](#)] [[PubMed](#)]
42. Daphedar, A.; Taranath, T.C. Green Synthesis of Zinc Nanoparticles Using Leaf Extract of *Albizia Saman* (Jacq.) Merr. and Their Effect on Root Meristems of *Drimia Indica* (Roxb.) Jessop. *Caryologia* **2018**, *71*, 93–102. [[CrossRef](#)]
43. Bai, B.; Nie, Q.; Zhang, Y.; Wang, X.; Hu, W. Cotransport of Heavy Metals and SiO₂ Particles at Different Temperatures by Seepage. *J. Hydrol.* **2021**, *597*, 125771. [[CrossRef](#)]
44. Yadav, V.K.; Gnanamoorthy, G.; Ali, D.; Bera, S.P.; Roy, A.; Kumar, G.; Choudhary, N.; Kalasariya, H.; Basnet, A. Cytotoxicity, Removal of Congo Red Dye in Aqueous Solution Using Synthesized Amorphous Iron Oxide Nanoparticles from Incense Sticks Ash Waste. *J. Nanomater.* **2022**, *2022*, 5949595. [[CrossRef](#)]
45. Siddiqui, S.I.; Allehyani, E.S.; Al-Harbi, S.A.; Hasan, Z.; Abomuti, M.A.; Rajor, H.K.; Oh, S. Investigation of Congo Red Toxicity towards Different Living Organisms: A Review. *Processes* **2023**, *11*, 807. [[CrossRef](#)]
46. Bharti, R.; Yadav, M.; Singh, A.; Kumari, P.; Nishad, J.H.; Gautam, V.S.; Kharwar, R.N. Evaluation of Congo Red Dye Decolorization and Degradation Potential of an Endophyte *Colletotrichum Gloeosporioides* Isolated from *Thevetia Peruviana* (Pers.) K. Schum. *Folia Microbiol.* **2023**, *68*, 381–393. [[CrossRef](#)]
47. Vinodhini, S.; Sengani, M.; Choudhury, A.A.; Ramasubbu, K.; Chakraborty, S.; Banerjee, M.; Balaji, M.P.; Devi Rajeswari, V. Regulation of Glucose Transporter-4 Intervention with *S. Saman* Leaves Extract in Streptozotocin-Induced Diabetic Rats. *J. Diabetes Complicat.* **2022**, *36*, 108340. [[CrossRef](#)]
48. Sajjad, H.; Sajjad, A.; Haya, R.T.; Khan, M.M.; Zia, M. Copper Oxide Nanoparticles: In Vitro and in Vivo Toxicity, Mechanisms of Action and Factors Influencing Their Toxicology. *Comp. Biochem. Physiol. Part C Toxicol. Pharmacol.* **2023**, *271*, 109682. [[CrossRef](#)]

49. Singleton, V.L.; Rossi, J.A. Colorimetry of Total Phenolics with Phosphomolybdic-Phosphotungstic Acid Reagents. *Am. J. Enol. Vitic.* **1965**, *16*, 144–158. [[CrossRef](#)]
50. Singleton, V.L.; Orthofer, R.; Lamuela-Raventós, R.M. [14] Analysis of Total Phenols and Other Oxidation Substrates and Antioxidants by Means of Folin-Ciocalteu Reagent. In *Methods in Enzymology*; Academic Press: Cambridge, MA, USA, 1999; Volume 299, pp. 152–178; ISBN 0076-6879.
51. Chang, C.-C.; Yang, M.-H.; Wen, H.-M.; Chern, J.-C. Estimation of Total Flavonoid Content in Propolis by Two Complementary Colorimetric Methods. *J. Food Drug Anal.* **2002**, *10*, 3.
52. Belwal, T.; Giri, L.; Bhatt, I.D.; Rawal, R.S.; Pande, V. An Improved Method for Extraction of Nutraceutically Important Polyphenolics from *Berberis Jaeschkeana* C.K. Schneid. Fruits. *Food Chem.* **2017**, *230*, 657–666. [[CrossRef](#)]
53. Johnston, J.W.; Dussert, S.; Gale, S.; Nadarajan, J.; Harding, K.; Benson, E.E. Optimisation of the Azinobis-3-Ethyl-Benzothiazoline-6-Sulphonic Acid Radical Scavenging Assay for Physiological Studies of Total Antioxidant Activity in Woody Plant Germplasm. *Plant Physiol. Biochem.* **2006**, *44*, 193–201. [[CrossRef](#)] [[PubMed](#)]
54. Brand-Williams, W.; Cuvelier, M.E.; Berset, C. Use of a Free Radical Method to Evaluate Antioxidant Activity. *LWT Food Sci. Technol.* **1995**, *28*, 25–30. [[CrossRef](#)]
55. Benzie, I.F.F.; Strain, J.J. The Ferric Reducing Ability of Plasma (FRAP) as a Measure of “Antioxidant Power”: The FRAP Assay. *Anal. Biochem.* **1996**, *239*, 70–76. [[CrossRef](#)]
56. Liu, W.; Zheng, J.; Ou, X.; Liu, X.; Song, Y.; Tian, C.; Rong, W.; Shi, Z.; Dang, Z.; Lin, Z. Effective Extraction of Cr(VI) from Hazardous Gypsum Sludge via Controlling the Phase Transformation and Chromium Species. *Environ. Sci. Technol.* **2018**, *52*, 13336–13342. [[CrossRef](#)] [[PubMed](#)]
57. Venugopal, A.; Arumugam, S.; Annamalai, S.; Jkkmmrf’s-Annai, N.; Sampoorani, J. In-Vitro Screening of Methanolic Leaf Extracts of *Albizia Saman* (Jacq.) Merr, for Their Antioxidant Property. *Int. J. Pharm. Health Care Res.* **2014**, *2*, 179–183.
58. Anil, A.; Nair, M.S.; Kumar, T.S. Phytochemical Analysis of Fruit Pulp of *Albizia Saman* (Jacq.) Merr, Fabaceae. *J. Pharmacogn. Phytochem.* **2018**, *7*, 2218–2220.
59. Alhalili, Z. Green Synthesis of Copper Oxide Nanoparticles CuO NPs from Eucalyptus Globoulus Leaf Extract: Adsorption and Design of Experiments. *Arab. J. Chem.* **2022**, *15*, 103739. [[CrossRef](#)]
60. Jacobs, H.; Moalin, M.; Bast, A.; van der Vijgh, W.J.F.; Haenen, G.R.M.M. An Essential Difference between the Flavonoids MonoHER and Quercetin in Their Interplay with the Endogenous Antioxidant Network. *PLoS ONE* **2010**, *5*, e13880. [[CrossRef](#)]
61. Nzilu, D.M.; Madivoli, E.S.; Makhanu, D.S.; Wanakai, S.I.; Kiprono, G.K.; Kareru, P.G. Green Synthesis of Copper Oxide Nanoparticles and Its Efficiency in Degradation of Rifampicin Antibiotic. *Sci. Rep.* **2023**, *13*, 14030. [[CrossRef](#)]
62. Caunii, A.; Pribac, G.; Grozea, I.; Gaitin, D.; Samfira, I. Design of Optimal Solvent for Extraction of Bio-Active Ingredients from Six Varieties of *Medicago Sativa*. *Chem. Cent. J.* **2012**, *6*, 123. [[CrossRef](#)]
63. Swathilakshmi, A.V.; Abirami, S.; Geethamala, G.V.; Poonkothai, M.; Sudhakar, C.; Albasher, G.; Alamri, O.; Alsultan, N. Phytanofabrication of Copper Oxide Mediated by *Albizia Amara* and Its Photocatalytic Efficacy. *Mater. Lett.* **2022**, *314*, 131911. [[CrossRef](#)]
64. Jayakumarai, G.; Gokulpriya, C.; Sudhapriya, R.; Sharmila, G.; Muthukumar, C. Phytofabrication and Characterization of Monodisperse Copper Oxide Nanoparticles Using *Albizia Lebbeck* Leaf Extract. *Appl. Nanosci.* **2015**, *5*, 1017–1021. [[CrossRef](#)]
65. Chauhan, A.; Verma, R.; Batoo, K.M.; Kumari, S.; Kalia, R.; Kumar, R.; Hadi, M.; Raslan, E.H.; Imran, A. Structural and Optical Properties of Copper Oxide Nanoparticles: A Study of Variation in Structure and Antibiotic Activity. *J. Mater. Res.* **2021**, *36*, 1496–1509. [[CrossRef](#)]
66. Verma, N.; Kumar, N. Synthesis and Biomedical Applications of Copper Oxide Nanoparticles: An Expanding Horizon. *ACS Biomater. Sci. Eng.* **2019**, *5*, 1170–1188. [[CrossRef](#)]
67. Amin, F.; Fozia; Khattak, B.; Alotaibi, A.; Qasim, M.; Ahmad, I.; Ullah, R.; Bourhia, M.; Gul, A.; Zahoor, S.; et al. Green Synthesis of Copper Oxide Nanoparticles Using *Aerva Javanica* Leaf Extract and Their Characterization and Investigation of *In Vitro* Antimicrobial Potential and Cytotoxic Activities. *Evid. Based Complement. Altern. Med.* **2021**, *2021*, 5589703. [[CrossRef](#)] [[PubMed](#)]
68. Sahoo, K.; Varshney, N.; Das, T.; Mahto, S.K.; Kumar, M. Copper Oxide Nanoparticle: Multiple Functionalities in Photothermal Therapy and Electrochemical Energy Storage. *Appl. Nanosci.* **2023**, *13*, 5537–5558. [[CrossRef](#)]
69. Yan, W.; Liu, D.; Tan, D.; Yuan, P.; Chen, M. FTIR Spectroscopy Study of the Structure Changes of Palygorskite under Heating. *Spectrochim. Acta A Mol. Biomol. Spectrosc.* **2012**, *97*, 1052–1057. [[CrossRef](#)]
70. Ramya, V.; Indhumathi, S.; Rajalakshmi, M.A.; Revathi, J.; Veeradarshini, E.; Sathyapriya, N. Facile Green Synthesis and Characterization Copper Oxide Nanoparticles Using *Albizia Amara* Leaves Extract. *Int. Res. J. Eng. Technol.* **2022**, *9*, 3236–3244.
71. Wang, L.; Du, Y.; Zhu, Q.; Song, J.; Ou, K.; Xie, G.; Yu, Z. Regulating the Alkyl Chain Length of Quaternary Ammonium Salt to Enhance the Inkjet Printing Performance on Cationic Cotton Fabric with Reactive Dye Ink. *ACS Appl. Mater. Interfaces* **2023**, *15*, 19750–19760. [[CrossRef](#)]
72. Hu, J.; Zhao, L.; Luo, J.; Gong, H.; Zhu, N. A Sustainable Reuse Strategy of Converting Waste Activated Sludge into Biochar for Contaminants Removal from Water: Modifications, Applications and Perspectives. *J. Hazard. Mater.* **2022**, *438*, 129437. [[CrossRef](#)] [[PubMed](#)]
73. Batool, M.; Qureshi, M.Z.; Hashmi, F.; Mehboob, N.; Shah, A.S. Congo Red Azo Dye Removal and Study of Its Kinetics by Aloe Vera Mediated Copper Oxide Nanoparticles. *Indones. J. Chem.* **2019**, *19*, 626–637. [[CrossRef](#)]

74. Jethave, G.; Fegade, U.; Inamuddin; Altalhi, T.; Khan, M.F.; Barhate, B.; Suryawanshi, K.E.; Isai, K.A. Adsorption of Congo Red Dye on CuO Nanoparticles Synthesized by Green Method Using Nyctanthes Arbor-Tristis Leaf Extract: Experimental and Theoretical Study. *Int. J. Chem. Kinet.* **2022**, *54*, 513–522. [[CrossRef](#)]
75. Rasheed, S.; Batool, Z.; Intisar, A.; Riaz, S.; Shaheen, M.; Kousar, R. Enhanced Photodegradation Activity of Cuprous Oxide Nanoparticles towards Congo Red for Water Purification. *Desalination Water Treat.* **2021**, *227*, 330–337. [[CrossRef](#)]
76. Harja, M.; Buema, G.; Bucur, D. Recent Advances in Removal of Congo Red Dye by Adsorption Using an Industrial Waste. *Sci. Rep.* **2022**, *12*, 6087. [[CrossRef](#)]
77. Said, M.I.; Othman, A.A.; Abd El Hakeem, E.M. Structural, Optical and Photocatalytic Properties of Mesoporous CuO Nanoparticles with Tunable Size and Different Morphologies. *RSC Adv.* **2021**, *11*, 37801–37813. [[CrossRef](#)]
78. Debnath, P.; Mondal, N.K. Effective Removal of Congo Red Dye from Aqueous Solution Using Biosynthesized Zinc Oxide Nanoparticles. *Environ. Nanotechnol. Monit. Manag.* **2020**, *14*, 100320. [[CrossRef](#)]
79. Kaur, S.; Rani, S.; Mahajan, R.K. Adsorption Kinetics for the Removal of Hazardous Dye Congo Red by Biowaste Materials as Adsorbents. *J. Chem.* **2013**, *2013*, 628582. [[CrossRef](#)]
80. Litefti, K.; Freire, M.S.; Stitou, M.; González-Álvarez, J. Adsorption of an Anionic Dye (Congo Red) from Aqueous Solutions by Pine Bark. *Sci. Rep.* **2019**, *9*, 16530. [[CrossRef](#)]
81. Jabbar, J.M.; Odusote, Y.A.; Alabi, K.A.; Ahmed, I.B. Kinetics and Mechanisms of Congo-Red Dye Removal from Aqueous Solution Using Activated Moringa Oleifera Seed Coat as Adsorbent. *Appl. Water Sci.* **2020**, *10*, 136. [[CrossRef](#)]
82. Amari, A.; Yadav, V.K.; Pathan, S.K.; Singh, B.; Osman, H.; Choudhary, N.; Khedher, K.M.; Basnet, A. Remediation of Methyl Red Dye from Aqueous Solutions by Using Biosorbents Developed from Floral Waste. *Adsorpt. Sci. Technol.* **2023**, *2023*, 1532660. [[CrossRef](#)]
83. Venkata, A.L.K.; Anthony, S.P.; Muthuraman, M.S. Synthesis of Solanum Nigrum Mediated Copper Oxide Nanoparticles and Their Photocatalytic Dye Degradation Studies. *Mater. Res. Express* **2019**, *6*, 125402. [[CrossRef](#)]
84. Krishna Kumar, A.S.; Warchol, J.; Matusik, J.; Tseng, W.L.; Rajesh, N.; Bajda, T. Heavy Metal and Organic Dye Removal via a Hybrid Porous Hexagonal Boron Nitride-Based Magnetic Aerogel. *NPJ Clean Water* **2022**, *5*, 24. [[CrossRef](#)]
85. Singh, P.; Singh, K.R.B.; Singh, J.; Das, S.N.; Singh, R.P. Tunable Electrochemistry and Efficient Antibacterial Activity of Plant-Mediated Copper Oxide Nanoparticles Synthesized by: Annona Squamosa Seed Extract for Agricultural Utility. *RSC Adv.* **2021**, *11*, 18050–18060. [[CrossRef](#)] [[PubMed](#)]
86. Chen, J.; Mao, S.; Xu, Z.; Ding, W. Various Antibacterial Mechanisms of Biosynthesized Copper Oxide Nanoparticles against Soilborne Ralstonia Solanacearum. *RSC Adv.* **2019**, *9*, 3788–3799. [[CrossRef](#)]
87. Nabila, M.I.; Kannabiran, K. Biosynthesis, Characterization and Antibacterial Activity of Copper Oxide Nanoparticles (CuO NPs) from Actinomycetes. *Biocatal. Agric. Biotechnol.* **2018**, *15*, 56–62. [[CrossRef](#)]
88. Iqbal, J.; Andleeb, A.; Ashraf, H.; Meer, B.; Mehmood, A.; Jan, H.; Zaman, G.; Nadeem, M.; Drouet, S.; Fazal, H.; et al. Potential Antimicrobial, Antidiabetic, Catalytic, Antioxidant and ROS/RNS Inhibitory Activities of Silybum Marianum Mediated Biosynthesized Copper Oxide Nanoparticles. *RSC Adv.* **2022**, *12*, 14069–14083. [[CrossRef](#)]
89. Bezza, F.A.; Tichapondwa, S.M.; Chirwa, E.M.N. Fabrication of Monodispersed Copper Oxide Nanoparticles with Potential Application as Antimicrobial Agents. *Sci. Rep.* **2020**, *10*, 16680. [[CrossRef](#)]
90. Derakhshani, E.; Asri, M.; Naghizadeh, A. Plant-Based Green Synthesis of Copper Oxide Nanoparticles Using Berberis Vulgaris Leaf Extract: An Update on Their Applications in Antibacterial Activity. *Bionanoscience* **2023**, *13*, 212–218. [[CrossRef](#)]
91. Vidovix, T.B.; Januário, E.F.D.; Araújo, M.F.; Bergamasco, R.; Vieira, A.M.S. Efficient Performance of Copper Oxide Nanoparticles Synthesized with Pomegranate Leaf Extract for Neutral Red Dye Adsorption. *Environ. Prog. Sustain. Energy* **2022**, *41*, e13864. [[CrossRef](#)]
92. Mohammed Ali, M.J.; Radhy, M.M.; mashkooor, S.J.; Ali, E.M. Synthesis and Characterization of Copper Oxide Nanoparticles and Their Application for Solar Cell. *Mater. Today Proc.* **2022**, *60*, 917–921. [[CrossRef](#)]

Disclaimer/Publisher's Note: The statements, opinions and data contained in all publications are solely those of the individual author(s) and contributor(s) and not of MDPI and/or the editor(s). MDPI and/or the editor(s) disclaim responsibility for any injury to people or property resulting from any ideas, methods, instructions or products referred to in the content.